National Physical Laboratory

NPL Report TQE 28

Calculations of the Fringing Capacitance of Cylindrical Electrodes

A P Gregory, T E Hodgetts, R N Clarke and G J Hill

NOVEMBER 2023

Calculations of the Fringing Capacitance of Cylindrical Electrodes

A. P. Gregory, T. E. Hodgetts*, R. N. Clarke and G. J. Hill*

*Consultant

Electromagnetic Technologies Group
Electromagnetic and Electrochemical Technologies Department

ABSTRACT

The accuracy of measurements of dielectric permittivity made with admittance cells and similar instruments is often limited by the effects of fringing-capacitance. These effects can be reduced by a physical approach that requires an additional electrode that is known as a guard ring, or by numerical corrections derived from calculations of the fringing capacitance. This report studies electrostatic calculations of fringing capacitance for a two-electrode capacitor consisting of a rod or disc that is enclosed by a longer surrounding cylinder or reentrant cylinder. The space between the ends of the electrodes is filled by air and an optional sheet of a uniform dielectric. Comparisons are made between calculations with several types software, including finite-element modelling, boundary-element modelling and mode matching. Corrections for the effects of fringing capacitance on measurements of permittivity by the Lynch method are derived for two radio-frequency instruments. For a Hartshorn and Ward apparatus resonant at 6 MHz, the corrections are found to improve measurement accuracy, but for a reentrant cavity resonant at 300 MHz they are not consistent with observations.

© NPL Management Limited, 2023

ISSN 1754-2995

https://doi.org/10.47120/npl.TQE28

National Physical Laboratory
Hampton Road, Teddington, Middlesex, TW11 0LW

This report is licensed under the Creative Commons CC-BY-ND 3.0 Licence
The full legal code is available at https://creativecommons.org/licenses/by-nd/3.0/

Approved on behalf of NPLML by R. A. Dudley,

Science Area Leader

CONTENTS

TABLES

FIGURES

CODE LISTINGS

ORGANISATION OF THIS REPORT

Section 1 introduces the main themes of this report: the fringing capacitance (C_f) between the end faces of two conducting discs or rods that are aligned on the same axis, and how to calculate it. It also describes its significance for measurements of the permittivity of laminar specimens made with instruments that use parallel-electrodes.

Section 2 describes parallel-electrode admittance cells and resonant systems for measuring the permittivity of sheets of material. Two resonance-based systems at NPL, a Hartshorn and Ward apparatus and a reentrant cavity, are described in detail in Section 2.3. Measurements with these systems are normally made by the Lynch equivalent-thickness (air-substitution) method described in Section 2.4.

Section 3 describes calculation of fringing capacitance by using mode-matching (program TEH2), the Boundary Element Method (program FastCap), and the Finite Element Method (program FEMM).

Section 4 compares TEH2, FastCap and FEMM capacitance calculations for air-spaced capacitors. Comparisons are also made against other sources of data, including results obtained from other programs.

Sections 5 and 6 describe how measurements of permittivity obtained by the Lynch method can be corrected for the effects of fringing fields. Corrections are calculated for the Hartshorn and Ward apparatus and the reentrant cavity respectively.

Measurements of the permittivity of a sheet of alumina with the Hartshorn and Ward apparatus, and the reentrant cavity are presented in Section 5.2 and Section 6.3. The measurements were made by the Lynch method. For both systems, the measured permittivity is observed to vary systematically as a function of the air gap between electrodes and specimen as a result of fringing-capacitance effects. The measurements are compared to predictions that are obtained from models for fringing capacitance.

Section 7 is the Conclusion.

Appendix A gives some technical details regarding the use of the FastCap program.

Appendices B.1 and B.2 present comparisons of C_f calculated by TEH2, FastCap and FEMM programs for a rod or disc electrode inside a cylinder, and a reentrant cylinder.

Appendix B.3 gives calculations of C_f for the electrode system used by the Hartshorn and Ward apparatus. These calculations were performed with FastCap and FEMM.

1 Introduction

The main theme of this report is calculation of the inter-electrode capacitance between the end-faces of parallel metal discs or rods that are aligned on the same axis. This can be characterised by two components: the *geometric capacitance* and the *fringing capacitance*. The application of this work is to enable measurements of the permittivity of laminar specimens made with parallel-electrode systems [1–3] to be corrected for the effects of fringing capacitance (which is a cause of measurement error). Methods for measuring permittivity will be described, and actual measurements with and without corrections for the effects of fringing capacitance will be compared to reference data.

The geometric capacitance of a parallel-plate capacitor with air dielectric is defined by $A\epsilon_a\epsilon_o/d$, where A is the area of the electrodes, d is their separation, ϵ_a is the relative permittivity of air, and ϵ_o is the *electric constant*[1]. The fringing capacitance is caused by charge accumulation near corners (for more information see the tutorial paper [4]). Figure 1 shows electrostatic electric-fields (E-fields) between two parallel disc-shaped electrodes that were calculated by using an FEM package, NGSolve[2]. The largest E-fields, shown in red, are almost entirely associated with geometric capacitance. Weaker fringing fields that occur between the edges and backs of the electrodes are shown in yellow and green. The fringing fields follow curved paths, although boundary conditions require them to meet the electrode surfaces at 90°. Fringing capacitance cannot be calculated precisely with simple formulae. In this report, computer software formulations that use different numerical methods of evaluating fringing capacitance are compared for a limited range of geometries. Such comparisons can be used to validate software to show that it is free from coding errors, so that improved traceability for calculated results can be obtained.

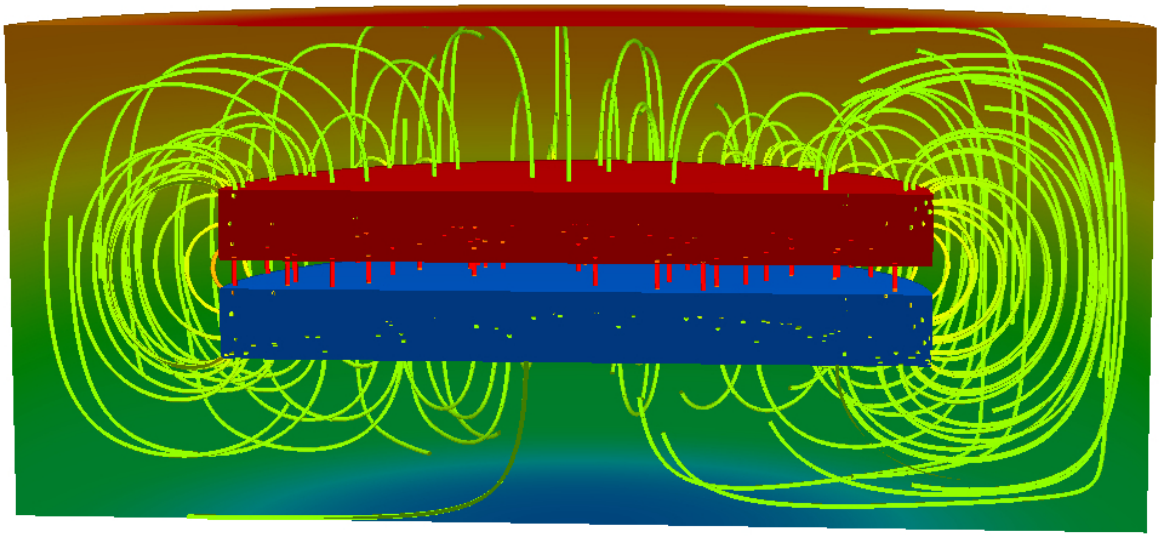

Figure 1: E-fields between disc-shaped electrodes at potentials ±0.5 V (cut along a diameter for illustration). The fields were calculated with an FEM package, NGSolve. The red lines represent the highest E-fields. Those shown in yellow and green represent much weaker fringing fields.

[1] Prior to the re-definition of the SI base units in 2019, this was usually referred to as *the permittivity of free space*.
[2] https://ngsolve.org/

The fringing capacitance of disc-shaped electrodes depends on their separation and on their aspect ratio (i.e. thickness / diameter). For a given electrode thickness, fringing capacitance increases approximately in proportion to the perimeter of the electrodes [5], i.e. $\sqrt{\text{Area}}$. The geometric capacitance is therefore a better approximation to the actual capacitance when the electrode area is large. Several papers present calculations of the fringing capacitance of electrodes that have infinitesimal thickness [4, 6, 7]. This report will only consider the much-less studied topic of rod-shaped (or "thick disc") electrodes.

2 Measurement of Dielectric Permittivity and Loss in Parallel-Electrode Systems

Techniques for measuring permittivity and loss in parallel-electrode systems fall into two main categories [3]:

- Admittance cell methods that use parallel-plate electrodes. LCR meters or Impedance Analysers are used provide a readout of capacitance and dissipation. *Two-terminal* and *three-terminal* admittance cells will be described.
- Resonance methods that use a Vector Network Analyser to measure resonant frequency and Q-factor. Parallel-plate electrodes can be resonated with a coil. Alternatively, rod-shaped electrodes can be fully enclosed to form a reentrant cavity.

2.1 Definitions

The *relative complex permittivity* of materials is given by $\epsilon^* = \epsilon' - \mathrm{j}\epsilon''$ where ϵ' and ϵ'' are positive quantities. In this report, the term *permittivity* is used to refer to the real part, ϵ'. The dielectric loss of materials is often represented by the *loss tangent* $\tan\delta = \epsilon''/\epsilon'$.

For low loss materials it is convenient to recognise that $\delta \approx \tan\delta$. The *loss angle*, δ, is often expressed in milliradians (mrad) or microradians (µrad). In this report, the term *low loss* is used when $\delta \lesssim 3\,\text{mrad}$, and *very low loss* is used when $\delta \lesssim 100\,\mu\text{rad}$. For materials that are used in microwave resonators and filters, it is common to refer to Q_f, which is given by $Q_f = 1/\delta$. For further discussion of these topics see reference [3].

2.2 Admittance cell/ LCR meter methods

Parallel-plate electrode systems for measurement of dielectric permittivity and loss [3] are usually equipped with a micrometer for setting the gap between the electrodes. The complete assembly of electrodes, supporting frame, and micrometer is sometimes referred to as a *dielectric test-set*. Various methods of performing these measurements have been proposed [8]. In this report, an equivalent-length method developed by A. C. Lynch (Section 2.4) is used.

2.2.1 Two-terminal cells

Figure 2a shows a two-terminal cell for measuring permittivity and loss angle. Permittivity and loss can be determined from measurements of capacitance and dissipation. These can be made by using an Impedance Bridge, but a modern automated instrument (LCR meter or Impedance Analyser) would normally be used nowadays. Commercial two-terminal cells, such as the Keysight 16453A test fixture [8], are available. The Keysight 16453A can be used at frequencies over 1 GHz in conjunction with a suitable Impedance Analyser.

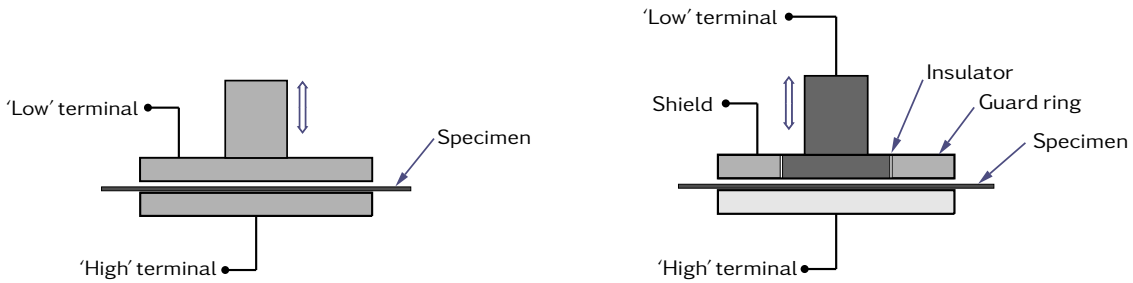

(a): Two terminal. **(b):** Three terminal.

Figure 2: Two-terminal and three-terminal cells for measurement of dielectric permittivity and loss.

Measurements of permittivity with two-terminal cells are prone to the effects of fringing capacitance, which can cause significant measurement error (typically 10 %). This report is primarily concerned with computational corrections based on calculations of the fringing capacitance of two-terminal electrode systems.

2.2.2 Three-terminal cells

Three terminal cells have an annular electrode (Figure 2b) known as a guard ring [9–11] which surrounds the low-potential electrode. These electrodes are electrically isolated by means of an insulator (air or a polymer such as PTFE), but are both nominally at ground potential. Measurements are made by using a four-terminal Impedance Bridge or a four-terminal LCR meter [12] that is connected to the electrodes by means of a four-terminal-pair configuration (four coaxial cables). The outer-screens of the four cables are connected to the guard ring, and the inner-conductors are connected to the appropriate electrodes with short wires. Series inductance associated with these connections limits the maximum frequency for accurate measurement. The guard ring and the low-potential electrode often have a knife-edge design [13]. This keeps the capacitance between them to a minimum, which improves the measurement sensitivity. The guard ring substantially reduces the effect of fringing fields on measurements when the separation between 'high' and 'low' electrodes is appreciably greater than the radial width of the insulator.

Three-terminal admittance cells are available from several manufacturers, including Keysight, Wayne Kerr and Solartron. Keysight model 16451B and Wayne Kerr model 1J1020 both use low-potential electrodes that are 38 mm diameter (corresponding to 10 pF capacitance between high- and low-potential electrodes at 1 mm separation) and have a maximum useful frequency of the order of 10 MHz.

2.3 Resonance methods

NPL possesses a number resonators can be used for measuring the permittivity and loss of sheets of low-loss and very low-loss materials. These are normally used in conjunction with Vector Network Analysers for measuring resonant frequency and Q-factor [14], from which permittivity and loss are calculated. This report will consider resonators that have parallel-plate electrodes (discs or rods) that can be adjusted with a micrometer to vary their separation. The measurement procedure used at NPL is the same as that used for admittance cells: the Lynch method (Section 2.4).

2.3.1 Resonance with a coil inductor (Hartshorn and Ward method)

The Hartshorn and Ward method uses a parallel-plate electrode system that is resonated with a coil inductor [15–17] (see Figure 3). The instrument at NPL, developed at ERA Technology, originally used series-resonance and an analogue Q-meter. It has recently been updated to use parallel resonance and a Vector Network Analyser [17]. Exchangeable coils enable resonances in the frequency range 1 – 70 MHz to be obtained. The enclosed geometry improves calculability and prevents the radiative effects that limit the precision of high-frequency measurements with unshielded electrodes. The ERA design uses a two-terminal electrode system. A three terminal instrument has been described by Kakimoto et al [13].

2.3.2 Reentrant cavities

Reentrant cavities [18–26] that operate at approximately 300 MHz and 600 MHz are available at NPL (see Figure 4). These are also known as Parry [27] or hybrid cavities, and are mostly used for measuring the loss of materials in the UHF range for which few other techniques are available. The reentrant design reduces the resonant frequency compared to a cylindrical cavity. Coupling loops placed in the coaxial section are used to excite resonances.

Electrostatic models given in this report can be used for calculating permittivity from measurements with reentrant cavities. Models based on TEM-mode propagation in which the cavity is represented by coaxial lines [22, 28] can also be used. To obtain the most accurate results, however, requires a 3D electromagnetic model [18, 20–22]. Mode matching techniques can be used to calculate the fields in the circular-waveguide section (a combination of TM_{01n} modes) and the fields in the coaxial-line section (TEM mode) according to the boundary conditions; hence permittivity can be be related to the resonant frequencies of the cavity. Barroso [23] used Finite Element Method (FEM) software (Poisson/Superfish [29]) for dielectric measurements with a reentrant cavity.

2.4 Measurement of permittivity and loss by the Lynch method

An equivalent-length (air-substitution) technique, known as the Lynch method [2, 3, 30], can be used for precise measurements of the permittivity and loss sheets of material with a dielectric test-set. Specimens to be measured are usually of sufficient size to extend beyond the region around the electrode edges where fringing fields are concentrated. A micrometer is used for adjustment of the separation of the electrodes. The procedure for measurement at one frequency is as follows: Inter-electrode capacitance is measured with the specimen to be measured *in situ*. A small air gap is left between the specimen and the top electrode (Figure 5) to avoid uncertainty associated with contact (from micrometer backlash, surface roughness & mechanical distortion of the electrode system). The specimen is removed and the separation of the electrodes is reduced to restore the capacitance or, for resonance methods, the resonant frequency. The permittivity is determined by using equation (1),

$$\epsilon' = \frac{t_s}{M_{\text{out}} - M_{\text{in}} + t_s} \,, \tag{1}$$

where t_s is the thickness of the dielectric sheet, and M_{in} and M_{out} micrometer readings with the specimen 'in' and 'out'. Traceability is via the calibration of the micrometer and so the measurements of capacitance (or resonant frequency) can be uncalibrated. They must, however, be (i) repeatable and (ii) independent of the dielectric loss of specimens. Furthermore, stray

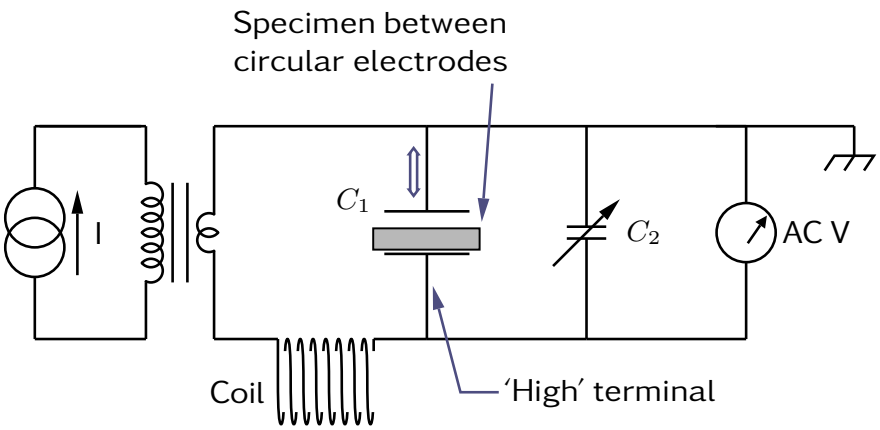

(a): Equivalent circuit.

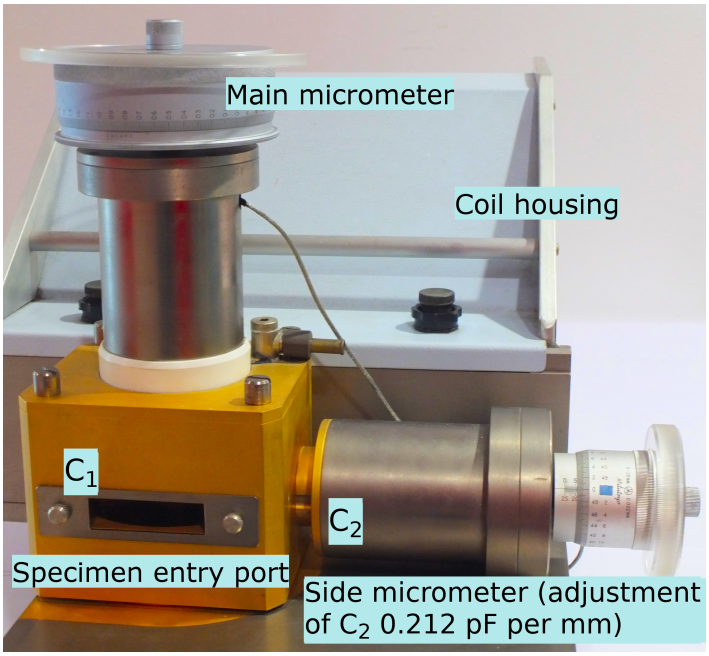

(b): Actual system manufactured by ERA Technology.

Figure 3: Hartshorn and Ward apparatus. Series or parallel resonant circuits can be used. The schematic shows a series resonance configuration that uses a low impedance drive from a step-down transformer. For measurement by using a Vector Network Analyser, a parallel resonance configuration without the transformer is used [17].

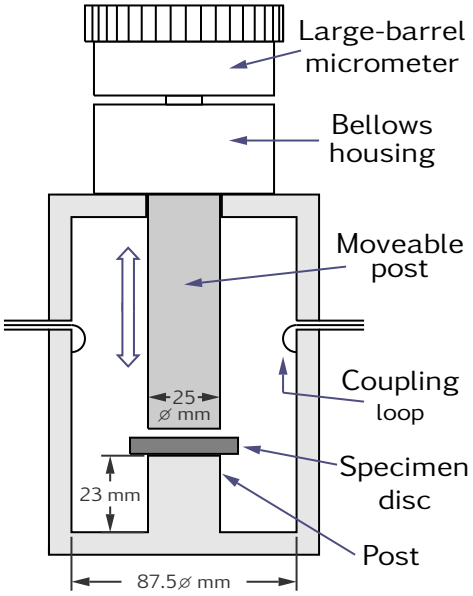

(a): Schematic.

(b): Photograph.

Figure 4: Reentrant cavity (designed by M. A. Barnett and G. J. Hill). The cavity shown has been used for measurements of dielectric loss at approximately 300 MHz [18]. The rectangular aperture visible in the photograph is the specimen entry port.

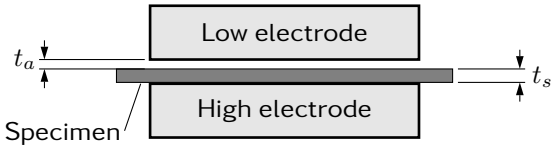

(a): Specimen 'in'.

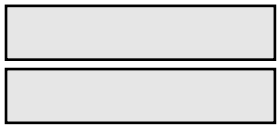

(b): Specimen 'out', capacitance restored.

Figure 5: Measurement by the Lynch method. A two- or three-terminal cell can be used.

capacitance external to the electrode system must be unchanged between the two measurements, although it does not need to be determined for measurement of permittivity.

For high-permittivity materials ($\epsilon' > 10$), the effect on measured ϵ' of uncertainty associated with the micrometer settings and the flatness and parallelism of electrodes and specimens can be very significant. By using specimens that have a smaller diameter than the electrodes, it is possible to reduce the uncertainty. This requires modified theory [16], and also requires the area of specimens and electrodes to be measured.

The dielectric loss angle is given by

$$\delta = (D_{\text{in}} - D_{\text{out}}) \times \frac{M_{\text{out}} - \Delta}{M_{\text{out}} - M_{\text{in}} + t_s} \tag{2}$$

where D_{in} and D_{out} are measurements of the dissipation of 'in' and 'out' measurements. Thus, traceable measurement of δ requires that the micrometer is calibrated, and that measurements of dissipation are obtained with a calibrated instrument. The quantity $D_{\text{in}} - D_{\text{out}}$ is the rotation of the phase angle of the impedance (in radians) between the measurements. In resonant systems, D_{in} and D_{out} are reciprocal Q-factors. The surface resistance of conductors is the same for the two measurements as they are made at the same frequency. If small changes in Q-factor can be resolved, δ can therefore be determined for very low loss materials [17].

The quantity Δ is the micrometer offset, defined as the reading when the electrodes are nominally in contact. Electrodes are seldom exactly parallel, but an effective value of Δ and an associated uncertainty can be estimated [17].

The term $(M_{\text{out}} - \Delta)\ /\ (M_{\text{out}} - M_{\text{in}} + t_s)$ accounts for *dilution* of the loss in the system by the layer of air between the electrode and specimen [30]. It is actually the ratio of the geometric capacitance of the specimen disc, $A\epsilon'\epsilon_o/t_s$ and the measured (assumed geometric) capacitance of air and specimen in combination. Further dilution occurs for Hartshorn and Ward apparatus because some of the resonant current flows through C_2 (marked in Figure 3) and through the stray capacitance. The effect of this on δ can be corrected for by consideration of the total capacitance in the system, and the calculated geometric and fringing components of the inter-electrode capacitance. An additional measurement enables the total capacitance to be determined [17].

2.4.1 The effect of fringing capacitance on measurements of ϵ'

For two-terminal electrode systems, ϵ' measured by the Lynch method is observed to be larger than expected, particularly when the air gap $(M_{\text{in}} - t_s)$ is large and for high-permittivity specimens. In other words, the micrometer displacement required to restore the capacitance after the specimen has been removed is greater than expected (i.e. the value of M_{out} is too small). Modelling shows that this is because the fringing capacitance C_f increases with permittivity

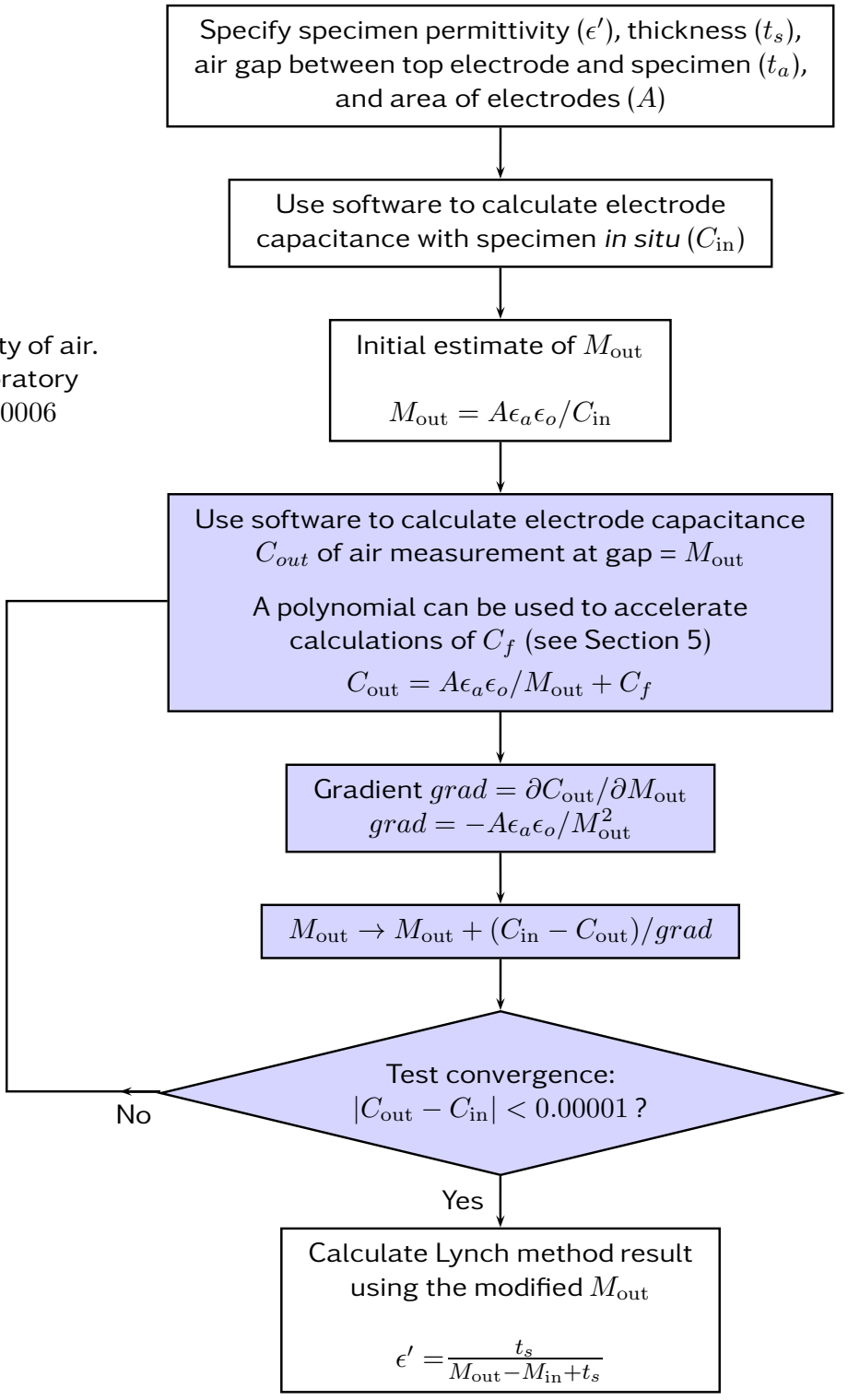

Figure 6: Process for predicting the *apparent* permittivity obtained by the Lynch method. The apparent permittivity for a two-terminal electrode system is higher than the actual permittivity because of the effect of fringing capacitance on $C_{\rm in}$ and $C_{\rm out}$. The predicted increase in the permittivity can be used to correct experimental data.

at a rate greater than the expected proportionality. An iterative process can be used to obtain corrections (Figure 6). This requires that C_f is calculated for both 'in' and 'out' measurements.

Guard rings (Section 2.2.2) can greatly reduce the effect of fringing capacitance, therefore avoiding the need for calculated corrections. These, however, become less effective if the electrode spacing is comparable to (or smaller than) the width of the insulator (Figure 2b). A useful rule-of-thumb for measurement by the Lynch method with three-terminal electrode systems is to perform the 'in' measurement with the vertical gap between the specimen and the uppermost electrode set to $\gtrsim 3\times$ the width of the insulator. This ensures that M_{out} cannot be too small.

3 Fringing Capacitance Calculations

Electrostatic calculation of the fringing capacitance of air-spaced parallel-plate electrodes is the subject of numerous papers, although the majority of these analyse "thin" electrodes [4, 6, 7]. These can find practical application for conducting foil, paint and evaporated metal electrodes [1]; the calculations in this report, however, are for unguarded rod-shaped and "thick disc" electrodes. Papers that consider "thick disc" electrodes include Lynch [5], Kamchouchi [31] and Scott [32] (who presents a formula that was proposed by Kirchhoff [33] in the nineteenth-century). Corrections to measurements of permittivity made by the equivalent-length method (Section 2.4) require fringing capacitance to be calculated when specimens are *in situ*. Lynch [5], estimated this by a graphical method based on equipotentials for a rectangular electrode that has the same perimeter as the disc-shaped electrodes of his experiment. These calculations were made assuming that the fringing capacitance / perimeter ratio is the same for both electrode shapes.

The fringing capacitance of the unshielded parallel-plate electrodes shown in Figure 5 is briefly considered in Section 4.4. This report, however, is predominantly concerned with calculations of the fringing capacitance of capacitors formed from concentric conducting cylinders. The reentrant cavity and the Hartshorn and Ward apparatus are taken as examples. Measurements of permittivity can be made in both of these systems by the Lynch method (and are subject to the effects of fringing capacitance), yet they are fundamentally different: the reentrant cavity is characterised by standing-wave resonances (albeit with fields concentrated in a narrow gap), whereas the electrode system in the Hartshorn and Ward apparatus is the capacitor in a resonant LC circuit. This report only considers electrostatic models. References to several papers on electromagnetic models for reentrant cavities are given in Section 2.3.2.

3.1 Mode matching: Programs TEH2 and TICELL

These two programs by Hodgetts use a coaxial line geometry in which the inner conductor is truncated perpendicular to the axis. They both use a mode-matching technique. For both programs, the frequency is an input parameter that can be in the GHz range (a practical limit arises because coaxial lines are not normally used overmoded). At MHz-frequencies and below, however, the dependence of the calculated C_f on the frequency is negligible. The data presented in this report is calculated at 1 MHz.

TEH2 Program TEH2 [34, 35] calculates the complex admittance $Y' + \mathrm{j}Y''$ at the discontinuity plane of an infinitely-long coaxial line terminated by a short-circuited circular waveguide filled by one or two dielectric layers as shown in Figure 7. TEH2 allows the diameters of the conductors of the coaxial line to change at the discontinuity plane, but this option is not needed for this work. The total capacitance between the truncated

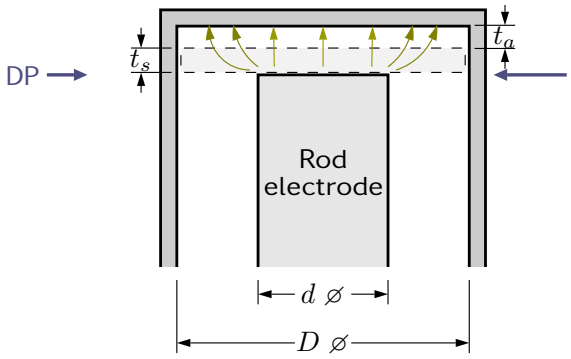

(a): Geometry

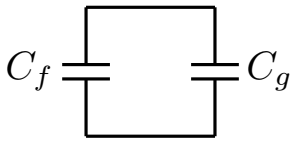

$$C_g = \frac{\epsilon'_{\text{eff}} \epsilon_o A}{t_a + t_s}$$

(b): Equivalent circuit
A = area of rod ends
ϵ'_{eff} is effective permittivity of air and specimen.

Figure 7: TEH2 calculation of fringing capacitance. Two layers (a dielectric specimen and air) above the discontinuity plane are shown, but the program can also be used when there is only one layer.

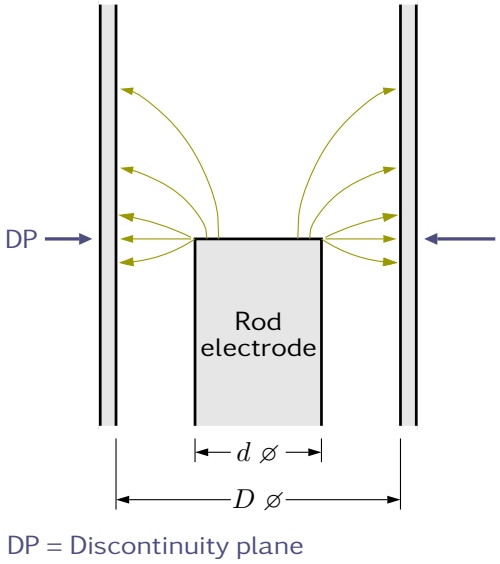

Figure 8: Coaxial line with discontinuous inner-conductor. C_f can be calculated by using program TICELL.

end of the inner conductor rod, and the side wall and short-circuited end of the circular waveguide, is Y''/ω (where $\omega = 2 \times \pi \times$ frequency). C_f is obtained by subtracting the geometric capacitance C_g between electrodes diameter d separated by a layer of air and a dielectric specimen. The full equation for C_f is

$$C_f = \frac{Y''}{\omega} - A\left(\frac{\epsilon_o\ \epsilon'_{\text{eff}}}{t_a + t_s}\right) \tag{3}$$

where t_a and t_s represent the thicknesses of the layer of air and the dielectric specimen respectively, and $A = \pi(d/2)^2$. If the specimen has low loss, the effective permittivity ϵ'_{eff} is given by

$$\epsilon'_{\text{eff}} = (t_a + t_s) \Big/ \left(\frac{t_a}{1.0006} + \frac{t_s}{\epsilon'}\right) \tag{4}$$

where the permittivity of air (ϵ'_a) is 1.0006, and the permittivity of the specimen is ϵ'.

TICELL Program TICELL [34] considers a coaxial line geometry in which the inner conductor is truncated as shown in Figure 8. The outer-conductor is extended to form a theoretically infinitely-long circular waveguide. TICELL calculates the complex admittance at the discontinuity plane, from which the fringing capacitance is easily derived. This geometry has been used to make traceable open-circuits for calibrating Vector Network Analysers [36].

As TEH2 and TICELL [34, 35] use a mode-matching technique, the accuracy of calculations improves as the number of modes N is increased. Quadratic extrapolation from calculations at N, $N/2$ and and $N/4$ is used to improve accuracy [35]. Tables 1 and 2 show C_f calculated by using TEH2 as a function of N when the short-circuited end of the outer conductor is offset from the end of the rod electrode by: (i) a thin (0.1 mm) air gap, and (ii) a thick (2 mm) disc of dielectric that has permittivity 10. All other results presented in this report were calculated with N=256, as this has been shown to be sufficient. When N=256, TEH2 requires approximately 1 second to calculate C_f on a current PC.

3.1.1 The end-to-end capacitance of long rods

Symmetry considerations enable TEH2 to be used to calculate the end-to-end capacitance between infinitely-long conducting rods (separation g) placed concentrically inside an air-filled conducting cylinder. If required, C_f can be obtained by subtracting the geometric capacitance between the rod ends, C_g. The geometry used by TEH2 (Figure 7) is attained in a hypothetical experiment in which a short-circuit (metal foil of negligible thickness) is introduced halfway between the rods – see Figure 9. The capacitance calculated by TEH2 (for a layer of air thickness $g/2$) is twice the end-to-end capacitance of the rods. Supplementary results (Appendix B.2.1) establish that FastCap calculations for a long rod-shaped electrode give comparable results to TEH2. This finding increases confidence in FastCap results for coaxial geometries.

TEH2 can also be used when the two infinitely-long rods of Figure 9 are separated by a disc of dielectric material that has the same diameter as the cylinder (D). The value of this is that dielectric measurements in a suitable measurement cell can be corrected for the effects of fringing capacitance simply and rapidly. Accurate corrections should be obtainable even if the diameter of the dielectric disc is smaller than D, provided that the disc is large enough to fill the region around the perimeter of the rods where fringing fields are concentrated. Accurate calculation of the end-to-end capacitance with TEH2 requires that the faces of the disc actually touch the rods.

Table 1: The fringing capacitance of the electrode geometry shown in Figure 7 calculated by using TEH2 for an air layer (thickness $t_a = 0.1$ mm). Tabulated as a function of the number of modes, N.

N	C_f (pF)
8	3.418
16	3.754
32	4.183
64	4.526
128	4.716
256	4.777
512	4.774

(a) TEH2 calculations

D	108 mm
d	50 mm
Layer	Air only
t_a	0.1 mm
ϵ'	1.0006
See also	Figure 27

(b) Data

Table 2: The fringing capacitance of the electrode geometry shown in Figure 7 calculated by using TEH2 for a dielectric layer (thickness $t_d = 2$ mm). Tabulated as a function of the number of modes, N.

N	C_f (pF)
8	7.759
16	8.353
32	8.427
64	8.433
128	8.437
256	8.435
512	8.417

(a) TEH2 calculations

D	108 mm
d	50 mm
Layer	Dielectric disc only
t_s	2 mm
ϵ'	10
See also	Figure 29

(b) Data

3.2 Boundary element method: Programs FastCap and COMSOL

The Boundary Element Method (BEM) allows the inter-electrode capacitances of an assembly of electrodes and dielectrics to be calculated by solution of Poisson's equation. It requires the surfaces of the dielectrics and conductors to be meshed. For a system that has N electrodes, $N \times N$ Maxwell Capacitance Matrix of inter-electrode capacitances can be obtained. The accuracy of calculated results can be expected to diminish as the number of electrodes is increased. *Adaptive mesh refinement* can be used to optimise the mesh density according to surface charge density.

FastCap This is an open-source program that was developed by Nabors and White at MIT [37, 38]. It is typically used for calculations on small-scale circuits, and has a reputation for high accuracy compared to other similar programs. Fast Multipole [39] methods are used to accelerate the computation. This involves using expansions to represent groups of mesh elements to reduce the number of calculations that must be performed. Calculations with FastCap are onerous to carry out as the user must provide meshed representations of conducting and dielectric surfaces. In the work described, surface meshing of metal and dielectric surfaces was accomplished by using netgen software. The topics of compiling (C language) and using FastCap, and preparing mesh files, are discussed in Appendix A.

Figure 11 shows a typical mesh for a rod electrode. The mesh size on the perimeter at the rods ends is indicated by the parameter h_1. To improve the accuracy of calculated results, a finer mesh is used near corners where the charge density is greatest. It was

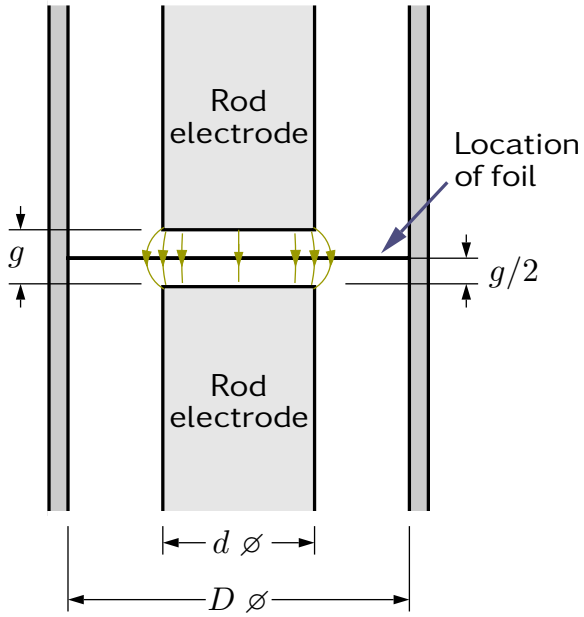

(a): Geometry

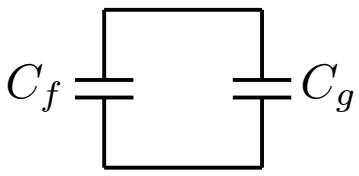

$$C_g = \frac{\epsilon_a \epsilon_o A}{g}$$

(b): Equivalent circuit
A = area of end rod ends
ϵ'_a = 1.0006

Figure 9: TEH2 Calculation of the end-to-end fringing capacitance between rods of infinite length inside a cylindrical shield.

found that making the mesh elements overly large in low-field regions (e.g. on the backs of disc electrodes) could cause FastCap to "hang". Adaptive Mesh Refinement is not supported by FastCap. The gradations in the mesh size shown in Figure 11 were informed by simulations made with NGSolve (discussed below) which does support adaptive mesh refinement.

COMSOL 5.5 (ESBE solver) COMSOL is a commercial multiphysics simulation package[3] that contains solvers for many types of problem. The Electrostatic Boundary-Element (ESBE) solver version 5.5 was used to determine the Maxwell Capacitance Matrix. Surface meshes were chosen to be similar to those used for FastCap.

3.3 Finite element method: Programs NGSOLVE and FEMM

The Finite Element Method (FEM) allows the inter-electrode capacitances of an assembly of electrodes and dielectrics to be calculated by solution of Poisson's equation.

FEMM 4.2 An open-source FEM solver[4] that is designed for axisymmetric and planar problems. It requires 2D meshing.

FEMM is comparatively rapid and efficient in its use of memory, so the mesh in every case could be made fine enough to ensure high accuracy (this was verified by changing the mesh size). It can be operated via a GUI or, if the package PyFEMM is installed, programmed via Python scripts.

[3] https://www.comsol.com/
[4] https://www.femm.info/wiki/HomePage

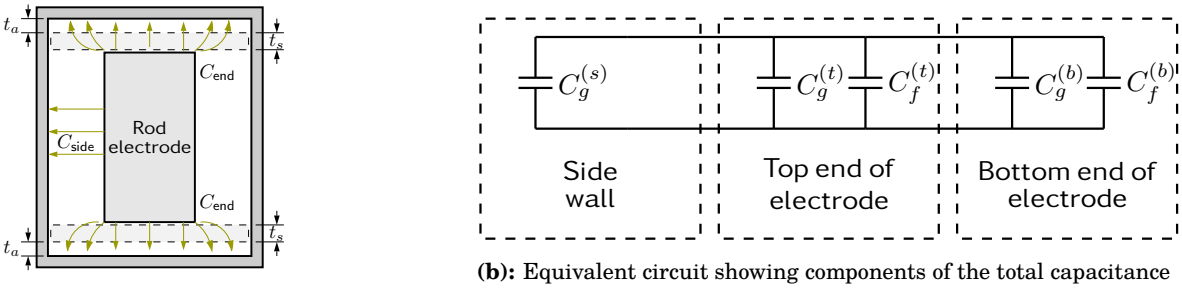

(a): Geometry

(b): Equivalent circuit showing components of the total capacitance (geometric C_g and fringing C_f).

Figure 10: Cylindrical geometry for calculation of fringing capacitance by using FastCap.

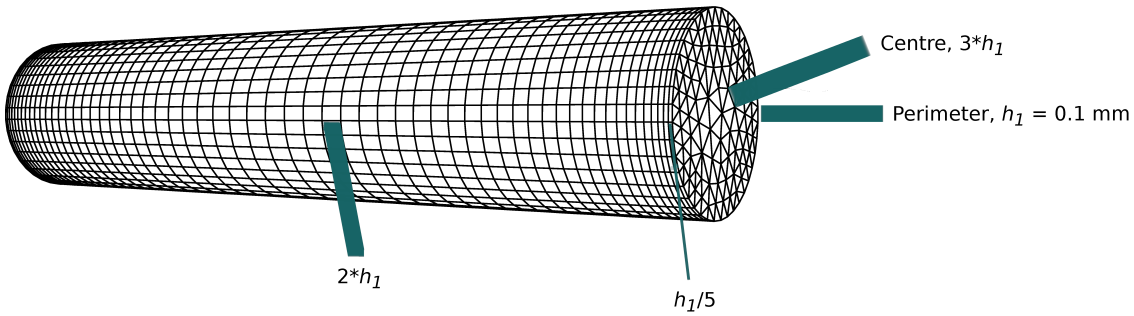

Figure 11: Meshing of rod electrode for FastCap. The mesh density is increased near the ends of the rod, where the charge density is highest. The parameter h_1 is the length of the side of mesh elements on the perimeter. The size of mesh elements elsewhere are in proportion to h_1 as marked. Reducing the size of h_1 generally improves accuracy, but also increases the amount of computer memory that is required.

NGSolve 6.2 An open-source FEM solver[5] that can be programmed with Python scripts. A tetrahedral 3D mesh with adaptive mesh refinement is used. The initial size of the mesh was chosen to allow solution using a computer with 32 GB of memory (range 0.25 – 0.5 mm).

3.4 Method of moments: Program SONNET

A commercial package[6] is designed for RF simulations of planar structures (e.g. microstrip and coplanar lines). It is possible to model disc-shaped electrodes that are coupled via microstrip lines (which are de-embedded). The finest available mesh setting was used to get the best accuracy. The frequency was specified as 1 MHz.

[5] https://ngsolve.org/
[6] https://www.sonnetsoftware.com/

4 Comparisons of Capacitance Calculations

In this section, capacitances calculated for air-spaced electrodes of spherical, coaxial and parallel-plate geometries with the software listed in Section 3 are compared. In all cases, the relative permittivity of air is taken to be 1.0006. For the parallel-plate geometry, comparisons the literature sources are made. Appendix B contains supplementary tables and graphs of fringing capacitance calculated with TEH2, FastCap and FEMM. Most of the results in this report were obtained by using a desktop computer with 32 GB of memory. This is ample for programs TEH2, TICELL and FEMM, but in some cases limits the accuracy for NGSolve and FastCap.

4.1 Concentric sphere geometry

The capacitance of concentric conducting spheres (Figure 12) is calculable, which makes this geometry a useful test case. If the spheres are separated by air, capacitance given by

$$C_{\mathrm{sph}} = 2\,\pi\,(1.0006)\,\epsilon_o\,D_1\,D_2/(D_2\;-\;D_1) \tag{5}$$

where D_1 and D_2 are the diameters of inner and outer spheres. This geometry is unique because all electric-field lines are straight.

Calculations made with FastCap and FEMM agree almost exactly with values obtained by using equation (5), even for small inter-electrode gaps – see Table 3. The meshed concentric spheres needed by FastCap were prepared by using functions in the netgen *constructive solid geometry* csg module. The mesh size was set to 0.25 mm for FastCap and to 'Auto' for FEMM.

Table 3: Tabulated values of the capacitance between concentric spheres.

D_1	D_2	C (pF)		
		FastCap	FEMM	Equation (5)
mm	mm	pF	pF	pF
6.0		0.835	0.835	0.835
7.0		1.299	1.299	1.299
8.0		2.227	2.227	2.227
9.0		5.010	5.010	5.010
9.6	10.0	13.359	13.360	13.360
9.7		17.999	17.999	17.999
9.8		27.278	27.280	27.276
9.9		55.111	55.111	55.109
9.95		110.780	110.776	110.775
9.99		556.090	556.102	556.102

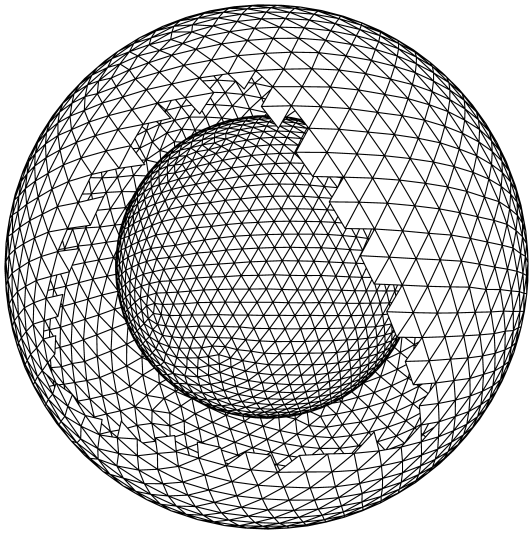

Figure 12: Meshed concentric-sphere capacitor.

4.2 Open-ended coaxial capacitor

The dimensions of the open-ended coaxial capacitor (Figure 13) are chosen so that fringing fields at the open ends of the outer conductor are negligible, which is a requirement for program TICELL. FastCap and COMSOL were used to calculate the total capacitance C_{total} from which C_f was calculated by using equations (6) and (7). The results (Table 4) are highly consistent. The conductor dimensions shown are those of 14 mm coaxial lines that are sometimes used in RF measurement [36]. C_f scales in proportion to the conductor diameters provided that their ratio $D/d = 2.303$ (corresponding to 50 Ω impedance) is maintained.

$$C_{\text{side}} = \frac{2\,\pi\,(1.0006)\,\epsilon_o\,\ell}{\ln\,(D/d)} \tag{6}$$

$$C_f = 0.5 \times (C_{\text{total}} - C_{\text{side}}) \tag{7}$$

4.3 Enclosed coaxial capacitor

The geometry shown in Figure 14 becomes equivalent to that in Figure 13 if L is comparable to, or greater than, D. Table 5 shows the results. The end capacitance, C_{end}, is the sum of the fringing capacitance, and the geometric capacitance between the ends of the inner and outer conductors. For D=14.288 mm, d=6.204 mm & L=15 mm the calculated value of C_{end} is the same as the fringing capacitance of the open-end geometry given in Table 4. As can be seen in Table 5, the agreement between the programs as a percentage of the total capacitance is, apart from one outlier, better than 0.1 % for wide range of radial gaps. TEH2 and FEMM results agree particularly well. Fringing capacitance data for a coaxial capacitor as a function of the gap between the end of the inner-conductor and the short-circuited end of the cylindrical cavity is given in Appendix B.1.1 (Figure 27 and Table 14).

Table 4: Tabulated values of fringing capacitance for the air-spaced open-ended coaxial capacitor shown in Figure 13.

D mm	d mm	L mm	C_f (pF) TICELL 32 Modes	C_f (pF) FastCap h_1=0.05 mm	C_f (pF) COMSOL ESBE 5.5
14.288	6.204	5.0		0.154	0.154
		10.0		0.161	0.161
		15.0		0.163	0.165
		∞	0.163		

Table 5: Tabulated values of the "end capacitance" for the enclosed coaxial capacitor shown in Figure 14.

D mm	d mm	L mm	C_{side} pF	C_{end} (pF) TEH2 128 Modes	C_{end} (pF) FastCap h_1=0.05 mm	C_{end} (pF) NGSolve Adaptive mesh	C_{end} (pF) FEMM Mesh 0.01 mm
14.288	6.204	5.0	0.667	0.173	0.173	0.173	0.173
		10.0	1.335	0.163	0.163	0.163	0.163
		15.0	2.002	0.163	0.163	0.163	0.163
10.000	6.000	15.0	3.269	0.177	0.176	0.178	0.177
	7.000		4.682	0.228	0.228	0.230	0.228
	8.000		7.484	0.301	0.301	0.303	0.301
	9.000		15.850	0.424	0.424	0.431	0.424
	9.600		40.909	0.588	0.598	0.604	0.588
	9.700		54.827	0.639	0.661	0.665	0.639
	9.800		82.661	0.712	0.775	0.753	0.712
	9.900		166.161	(Fails)	1.089	0.921	0.838

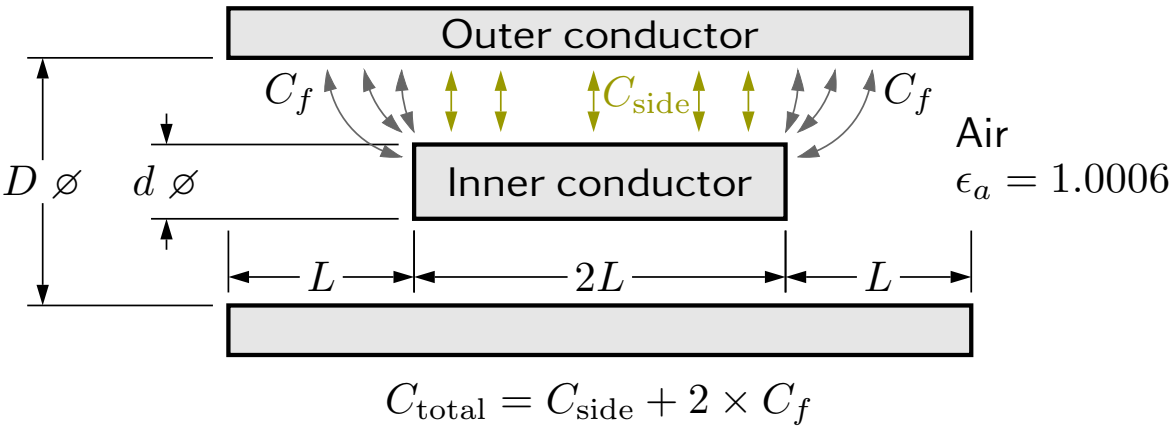

(a): Schematic diagram

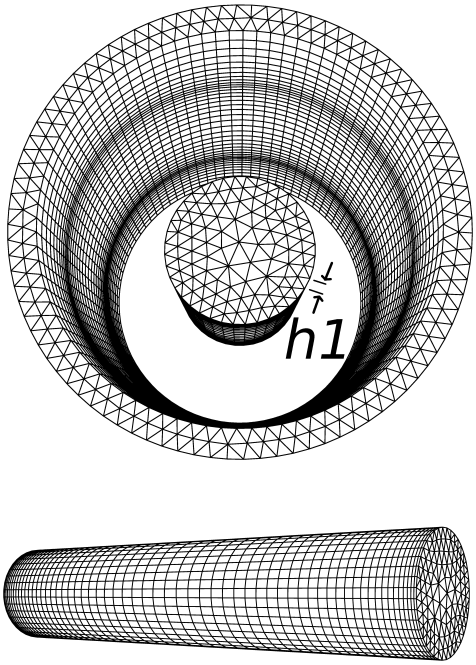

(b): FastCap mesh

Figure 13: Coaxial capacitor with open ends.

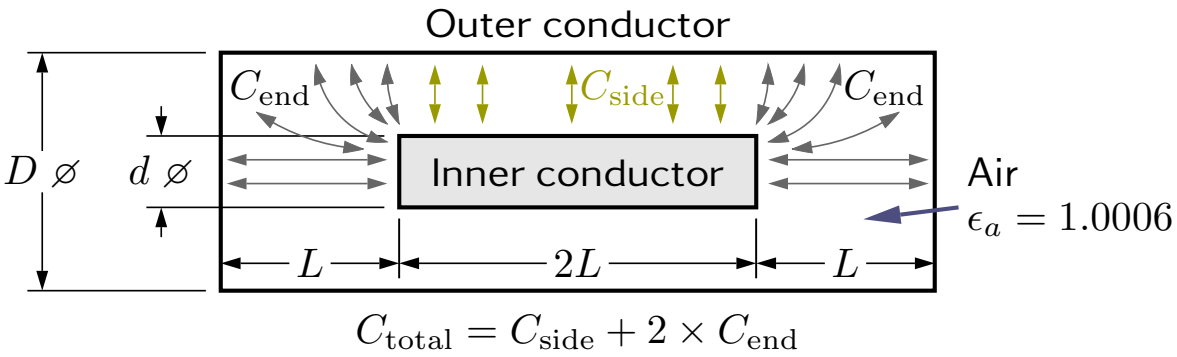

(a): Schematic diagram

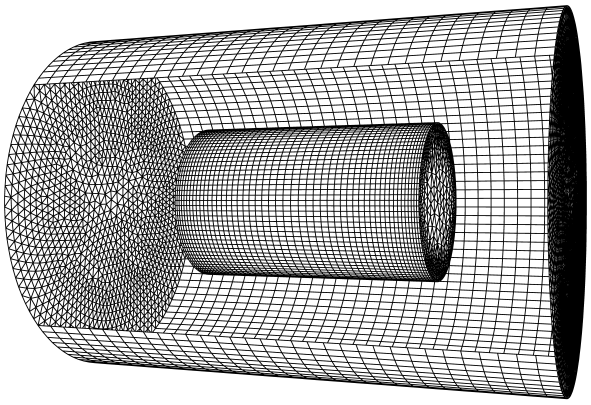

(b): FastCap mesh

Figure 14: Enclosed coaxial capacitor.

4.4 Capacitor with disc-shaped electrodes

Accurate measurement of permittivity by using two-terminal admittance cells (Figure 5) requires corrections to be made for the effects of fringing capacitance. Thus, calculations of the fringing capacitance between disc-shaped electrodes are needed with and without sheets of dielectric material between them [5].

The capacitance between "thick disc" electrodes (air spaced) was modelled with FastCap, COMSOL, SONNET and FEMM. The SONNET[7] and FEMM models placed the discs in a large conducting box – see Figures 15 and 16. FastCap and COMSOL (ESBE solver) are truer to the actual geometry as a boundary surrounding the electrodes is not required.

Table 6 compares fringing capacitance data for air-spaced discs 50ø×5 mm from the three programs and two literature sources. For this geometry, E-fields are not confined by a surrounding conductor (except for the large box in the SONNET model). FastCap data agrees well with the Kirchhoff formula [32, 33], and is consistent with the two 1970s literature sources to within approximately 15%. FEMM and COMSOL agree to within 5–10 %, but produce significantly higher results than FastCap and the Kirchhoff formula. The discrepancies observed are larger than those obtained for coaxial capacitors (Tables 4 and 5). It might be speculated that the effect of approximations, such as the multipole expansions used by FastCap, is increased for unbounded problems.

Table 6: Tabulated values of the fringing capacitance of air-spaced conducting discs, 50ø×5 mm.

	C_f (pF)						
	Literature values			This report			
Gap mm	Kirchhoff Formula [32]	Lynch [5]	Kamchouchi [31]	FastCap $h_1 = 0.05$ mm	FEMM	COMSOL ESBE 5.5	SONNET
0.5	1.811	2.16	2.172	1.926	2.552	2.695	2.222
1.0	1.514	1.84	1.883	1.629	2.223	2.282	2.017
2.0	1.226	1.53	1.595	1.356	1.979	2.199	1.811

[7] Support from Shrikrishna Hegde and Brian Rautio of Sonnet Software Inc. is gratefully acknowledged

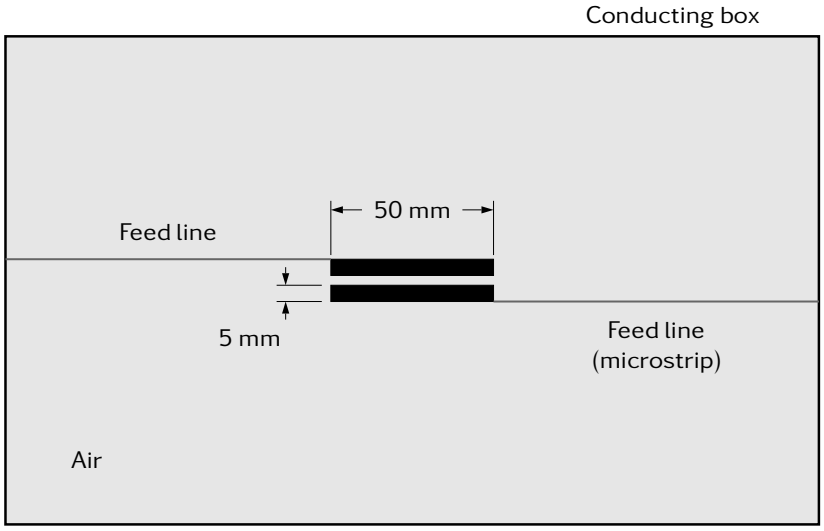

Figure 15: SONNET model for the disc capacitor (side view). The feed lines are de-embedded.

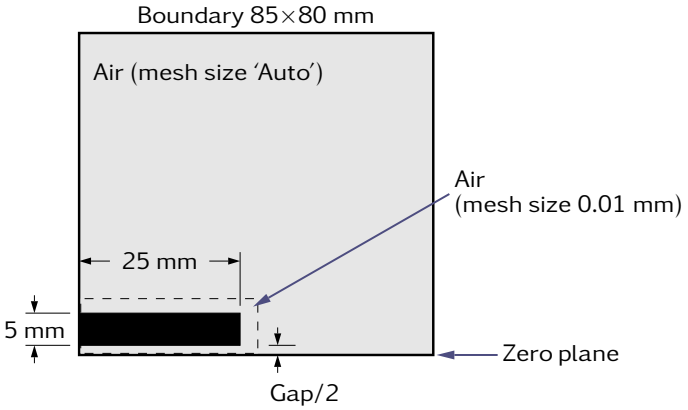

Figure 16: FEMM model for the disc capacitor (side view). As an axisymmetric representation is used, only the top-right quadrant is needed.

5 Corrections for the Effects of C_f on Lynch-Method Measurements of ϵ' by the Hartshorn and Ward Method

The calculations in this report show that the fringing capacitance of parallel electrode systems increases with specimen permittivity. A linear increase in proportion to permittivity is equivalent to using a slightly larger electrode, and should not affect measurements of permittivity by the Lynch method. A non-proportional dependence of fringing capacitance on permittivity will, however, cause measurement error. If the real part of the permittivity (ϵ'), specimen thickness (t_s) and the air gap between specimen and top electrode ($t_a = M_{\text{out}} - t_s - \Delta$) are specified, the *apparent* permittivity can be calculated by using the process outlined in Figure 6. Correction tables for measurements by the Lynch method can be therefore obtained. FastCap was used for the calculations presented, but FEMM could be used if the specimens (rectangles) are approximated as discs to give an axisymmetric geometry (Appendix B.3.2).

5.1 FastCap models

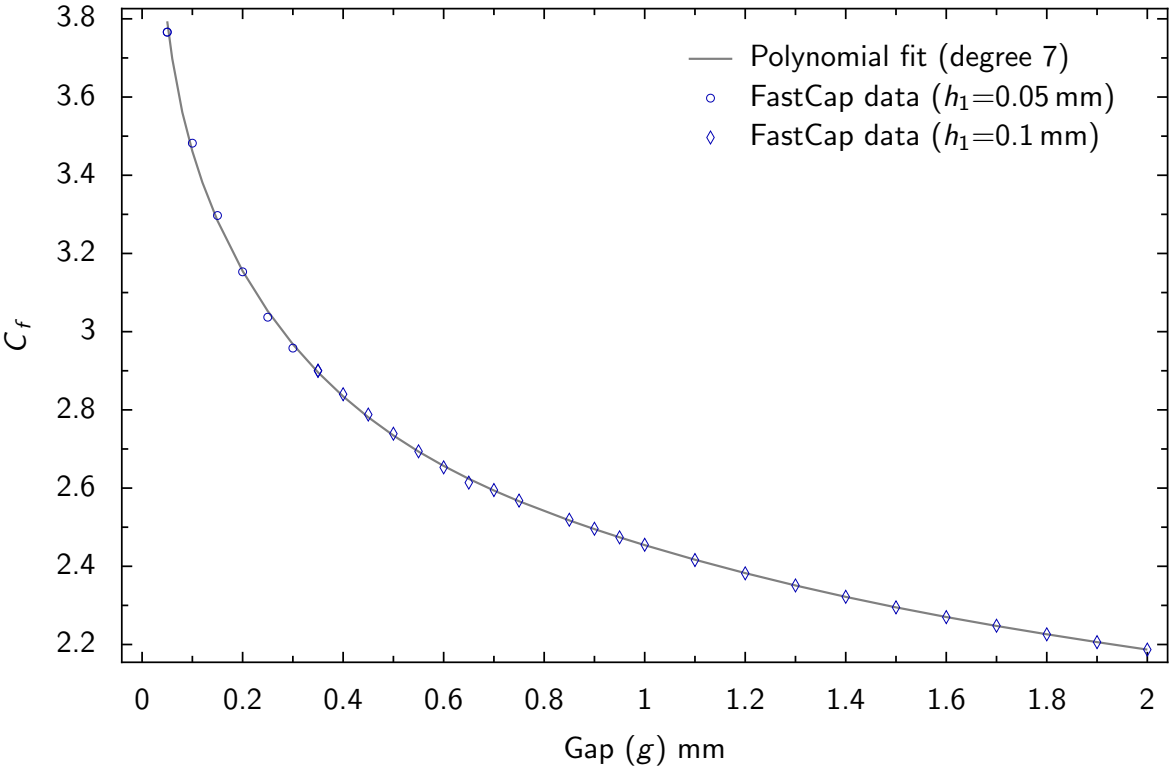

Figure 17: Polynomial fit of C_f as a function of air gap (no specimen) for the Hartshorn and Ward apparatus (geometry shown in Figure 18). The FastCap data is from Table 20. The parameter h_1 is the mesh size on the perimeter of the electrodes (see Figure 11).

The iterative model that will be presented requires calculations of fringing capacitance for the 'empty' measurement (i.e. on air) for varying gaps. To accelerate these calculations, fringing capacitance as a function of gap g is fitted by a polynomial. Figure 17 shows data points from Table 20 and the fitted polynomial, eqn. (8). The values of the coefficients are given in Table 7.

$$g \times C_f = a_0 + a_1 \times g + a_2 \times g^2 + a_3 \times g^3 + a_4 \times g^4 + a_5 \times g^5 + a_6 \times g^6 + a_7 \times g^7 \quad (8)$$

Table 7: Polynomial coefficients of fringing capacitance C_f (pF) of the Hartshorn and Ward electrode system as a function of air gap between electrodes (mm). The values shown were fitted to FastCap calculations of fringing capacitance for gaps in the range 0.05 mm to 2 mm. Refer to equation (8).

Coefficient	Value
a_0	0.020 713 22
a_1	3.523 600 78
a_2	−3.092 990 43
a_3	4.352 658 39
a_4	−3.819 781 16
a_5	1.927 738 91
a_6	−0.513 851 17
a_7	0.056 031 27

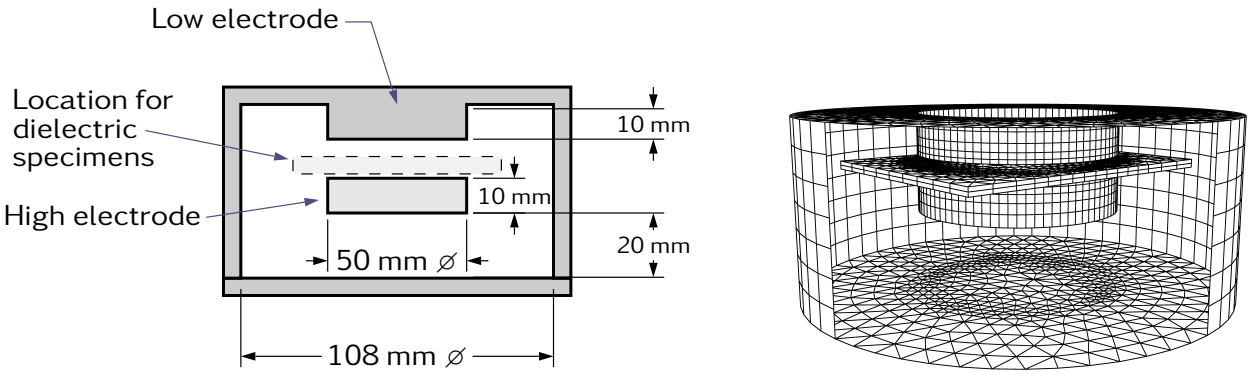

(a): Simplified geometry

(b): Mesh

Figure 18: Meshing for the Hartshorn and Ward electrode system with a rectangular specimen. This was used for calculating the results shown in Figure 17 with FastCap.

Table 8 shows a comparison between fringing capacitance calculated from the coefficients shown in Table 7, and values calculated directly by TEH2 (Section 3.1.1). Good agreement is not obtained because the electrodes have insufficient length for accurate modelling by using TEH2 (which is based on the assumption that the electrodes are rods that have practically infinite length).

Figure 19 shows plots of predictions of the apparent permittivity (i.e. the expected experimental results) as a function of the actual permittivity for a rectangular specimen 70 × 54 × 2 mm. The meshing scheme used is shown in Figure 18. The data is re-plotted in Figure 20a to show the increase in permittivity that is caused by uncorrected fringing capacitance effects. The calculations were repeated for a specimen of dimensions 70 × 54 × 1 mm (Figure 20b). These graphs show that if the air gap t_a between the top electrode and the specimen is small, the effect of fringing capacitance on measurements is significantly reduced. The corrections plotted in these graphs are tabulated in Tables 9 and 10 for specimens 2 mm and 1 mm thick. For convenience, the corrections can with reasonable accuracy be represented by simple equations [17].

Table 8: Comparison of fringing capacitance calculations for the Hartshorn and Ward electrode system shown in Figure 18 as a function of the air gap between electrodes. The FastCap values were obtained from the polynomial coefficients listed in Table 7. The TEH2 values were calculated as described in Section 3.1.1. Good agreement is not obtained because TEH2 requires that the electrodes are long rods.

Gap (mm)	C_f (mm)	
	FastCap	TEH2
0.10	3.461	2.705
0.20	3.155	2.388
0.50	2.735	1.966
1.00	2.454	1.659
2.00	2.187	1.362

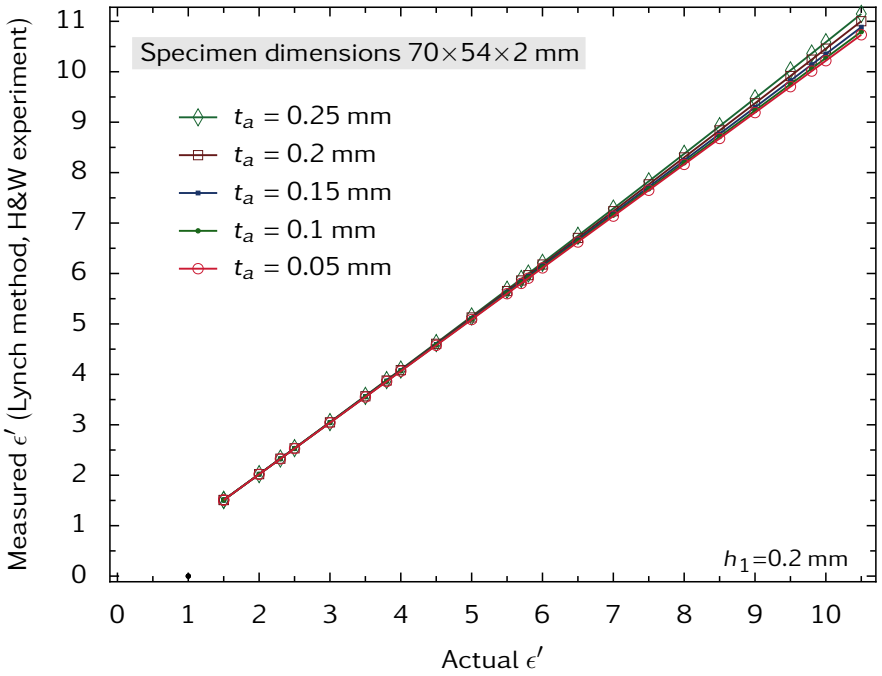

Figure 19: Calculations of apparent permittivity as a function of actual permittivity for Lynch method measurements in the Hartshorn and Ward apparatus. The apparent permittivity is higher than the actual permittivity as a result of the effects of fringing capacitance. The method of calculation is described in Figure 6 on page 8. FastCap was used for calculations of fringing capacitance.

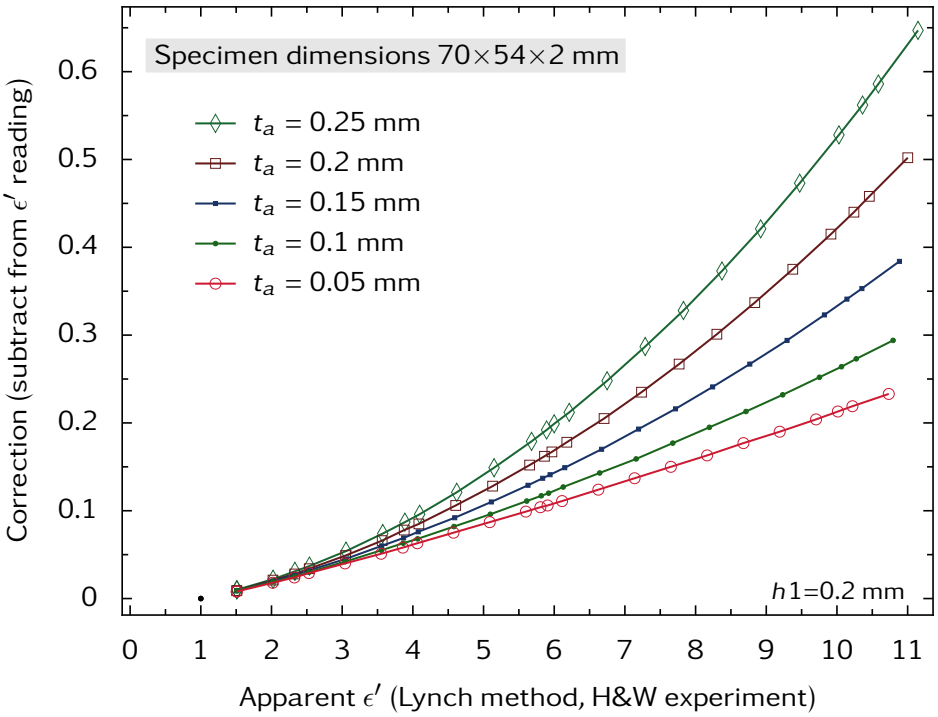

(a): Specimen dimensions 70×54×2 mm

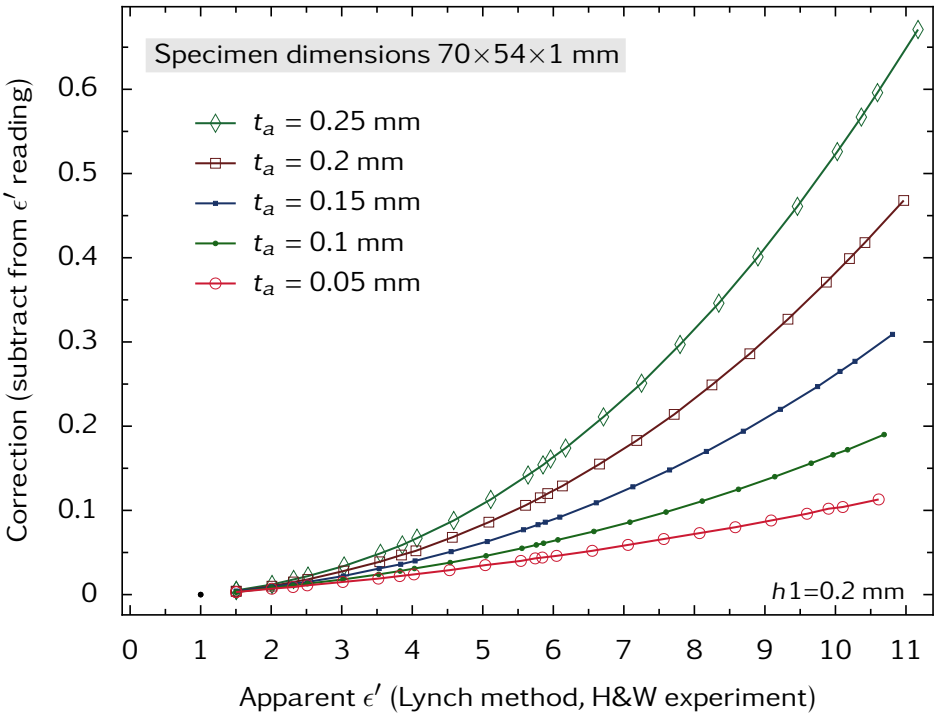

(b): Specimen dimensions 70×54×1 mm

Figure 20: Permittivity corrections for measurements in the Hartshorn and Ward apparatus. The Y-axis shows the size of the increase in ϵ' caused by fringing capacitance. Figure 20a shows the same data as Figure 19.

Table 9: Tabulated corrections to the permittivity ϵ'_{app} measured by the Lynch method for the Hartshorn and Ward apparatus. Measurements can be corrected by subtracting the appropriate table entry. Calculated for a rectangular specimen dimensions 70×54 mm that is **2 mm thick**. The mesh-size parameter h_1 for the FastCap calculations of C_{in} was 0.2 mm.

Air gap above specimen (t_a) in mm									
0.05		0.1		0.15		0.2		0.25	
ϵ'_{app}	Corr	ϵ'_{app}	Corr	ϵ'_{app}	Corr	ϵ'_{app}	Corr	ϵ'_{app}	Corr
1.508	0.008	1.509	0.009	1.509	0.009	1.509	0.009	1.510	0.010
2.018	0.018	2.019	0.019	2.020	0.020	2.021	0.021	2.022	0.022
2.324	0.024	2.325	0.025	2.327	0.027	2.328	0.028	2.331	0.031
2.529	0.029	2.530	0.030	2.532	0.032	2.534	0.034	2.537	0.037
3.040	0.040	3.042	0.042	3.045	0.045	3.049	0.049	3.054	0.054
3.551	0.051	3.555	0.055	3.560	0.060	3.566	0.066	3.574	0.074
3.858	0.058	3.863	0.063	3.869	0.069	3.878	0.078	3.887	0.087
4.063	0.063	4.068	0.068	4.076	0.076	4.085	0.085	4.096	0.096
4.575	0.075	4.582	0.082	4.592	0.092	4.606	0.106	4.621	0.121
5.087	0.087	5.096	0.096	5.110	0.110	5.128	0.128	5.149	0.149
5.599	0.099	5.611	0.111	5.629	0.129	5.652	0.152	5.679	0.179
5.804	0.104	5.817	0.117	5.837	0.137	5.862	0.162	5.892	0.192
5.906	0.106	5.920	0.120	5.941	0.141	5.967	0.167	5.999	0.199
6.111	0.111	6.127	0.127	6.149	0.149	6.178	0.178	6.212	0.212
6.624	0.124	6.643	0.143	6.670	0.170	6.705	0.205	6.748	0.248
7.137	0.137	7.159	0.159	7.193	0.193	7.235	0.235	7.287	0.287
7.650	0.150	7.677	0.177	7.716	0.216	7.767	0.267	7.828	0.328
8.163	0.163	8.195	0.195	8.241	0.241	8.301	0.301	8.373	0.373
8.677	0.177	8.713	0.213	8.767	0.267	8.837	0.337	8.921	0.421
9.190	0.190	9.232	0.232	9.294	0.294	9.375	0.375	9.473	0.473
9.704	0.204	9.752	0.252	9.823	0.323	9.915	0.415	10.028	0.528
10.013	0.213	10.064	0.264	10.141	0.341	10.240	0.440	10.362	0.562
10.219	0.219	10.273	0.273	10.353	0.353	10.458	0.458	10.586	0.586
10.733	0.233	10.794	0.294	10.884	0.384	11.002	0.502	11.147	0.647

Table 10: Tabulated corrections to the permittivity ϵ'_{app} measured by the Lynch method for the Hartshorn and Ward apparatus. Measurements can be corrected by subtracting the appropriate table entry. Calculated for a rectangular specimen dimensions 70×54 mm that is **1 mm thick**. The mesh-size parameter h_1 for the FastCap calculations of C_{in} was 0.2 mm.

Air gap above specimen (t_a) in mm									
0.05		0.1		0.15		0.2		0.25	
ϵ'_{app}	Corr	ϵ'_{app}	Corr	ϵ'_{app}	Corr	ϵ'_{app}	Corr	ϵ'_{app}	Corr
1.503	0.003	1.503	0.003	1.504	0.004	1.504	0.004	1.505	0.005
2.007	0.007	2.008	0.008	2.009	0.009	2.010	0.010	2.012	0.012
2.309	0.009	2.311	0.011	2.313	0.013	2.315	0.015	2.318	0.018
2.511	0.011	2.513	0.013	2.515	0.015	2.518	0.018	2.522	0.022
3.015	0.015	3.018	0.018	3.022	0.022	3.028	0.028	3.034	0.034
3.519	0.019	3.524	0.024	3.531	0.031	3.539	0.039	3.549	0.049
3.822	0.022	3.828	0.028	3.836	0.036	3.847	0.047	3.859	0.059
4.024	0.024	4.031	0.031	4.040	0.040	4.052	0.052	4.067	0.067
4.529	0.029	4.538	0.038	4.551	0.051	4.568	0.068	4.588	0.088
5.035	0.035	5.046	0.046	5.063	0.063	5.086	0.086	5.113	0.113
5.540	0.040	5.555	0.055	5.577	0.077	5.606	0.106	5.642	0.142
5.743	0.043	5.759	0.059	5.783	0.083	5.815	0.115	5.854	0.154
5.844	0.044	5.861	0.061	5.886	0.086	5.920	0.120	5.961	0.161
6.046	0.046	6.065	0.065	6.092	0.092	6.129	0.129	6.174	0.174
6.552	0.052	6.575	0.075	6.609	0.109	6.655	0.155	6.711	0.211
7.059	0.059	7.086	0.086	7.128	0.128	7.183	0.183	7.251	0.251
7.566	0.066	7.598	0.098	7.648	0.148	7.714	0.214	7.797	0.297
8.073	0.073	8.111	0.111	8.170	0.170	8.249	0.249	8.346	0.346
8.580	0.080	8.625	0.125	8.694	0.194	8.786	0.286	8.901	0.401
9.088	0.088	9.140	0.140	9.220	0.220	9.327	0.327	9.461	0.461
9.596	0.096	9.656	0.156	9.747	0.247	9.871	0.371	10.026	0.526
9.902	0.102	9.966	0.166	10.065	0.265	10.199	0.399	10.367	0.567
10.104	0.104	10.172	0.172	10.277	0.277	10.418	0.418	10.596	0.596
10.613	0.113	10.690	0.190	10.809	0.309	10.968	0.468	11.171	0.671

5.2 Experimental results

Lynch-method measurements of the permittivity of a specimen of alumina ($70 \times 54 \times 2.009$ mm), uncorrected for the effects of fringing capacitance, were obtained as a function of the air gap t_a between the specimen and the top electrode. These are compared to values predicted by models. The permittivity of the specimen is 9.68 with uncertainty 0.03 at k=2. This was measured at 2.45 GHz by using a Split-Post Dielectric Resonator [40]. As the material is very low loss, its permittivity will not be significantly greater at the lower frequencies used in the experiments described in this report (see discussion of the Lynch formula in reference [3])

Figure 21 shows a comparison between measurements of the permittivity by the Lynch method and values predicted by a FastCap model for the Hartshorn and Ward apparatus as a function of t_a. The uncertainty of measurement results is predominantly attributable to the specimen thickness uncertainty (0.004 mm at k=2). For high permittivity specimens, Lynch method results are very sensitive to dimensional uncertainty. There is insufficient data for a rigorous estimate of the uncertainties of the calculated values of C_f, but an estimated 'uncertainty corridor' is plotted. This is calculated for an uncertainty of $\Delta C = \pm 0.2$ pF where ΔC is the uncertainty of the change in the calculated fringing capacitance between 'in' and 'out' measurements. FastCap results for the contacting point (t_a=0) are calculated with a different meshing arrangement from that of the other FastCap results (as there is no intervening layer of air between top electrode and the specimen).

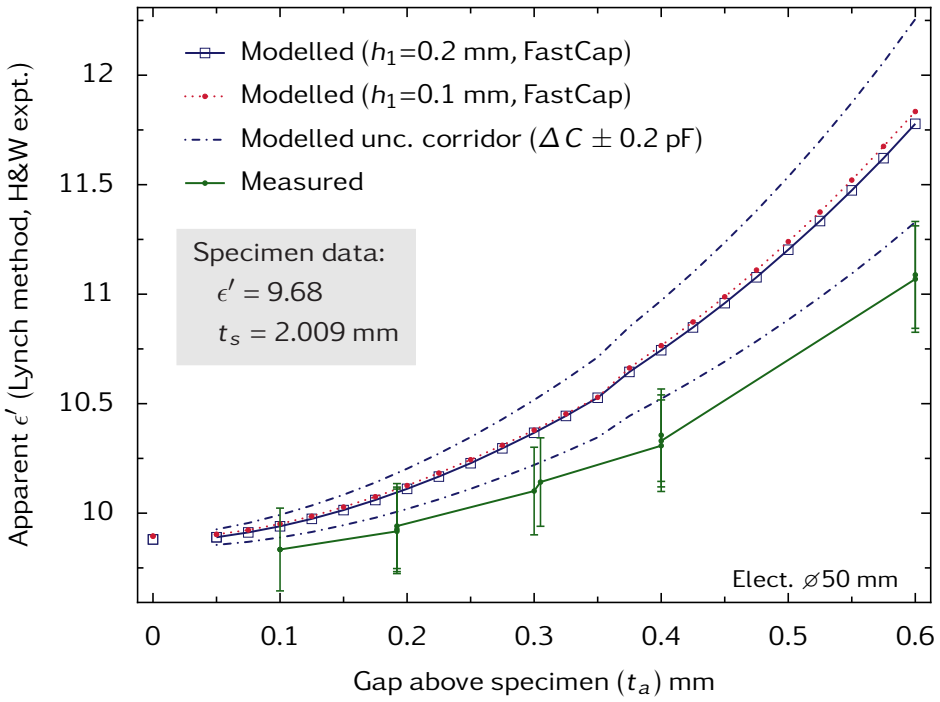

Figure 21: Measurements of ϵ' by the Lynch method as a function of the air gap above the specimen made with the Hartshorn & Ward apparatus at 6 MHz. Modelled values are also shown. The observed dependence of ϵ' on t_a is a consequence of fringing capacitance, for which no corrections are applied. The specimen was a rectangle of alumina, dimensions $70 \times 54 \times 2.009$ mm. The uncertainties of the experimental data are shown for a coverage factor of $k = 2$.

There are a number of observations that can be made about the results shown in Figure 21:

- Modelled and experimental results have a similar shape, both showing a rapid rise in ϵ' with increasing air gap between top electrode and specimen. Keeping the gap as small as possible is clearly advantageous, especially for a high-permittivity material.
- The apparent permittivity of the alumina specimen is higher than its actual permittivity at all gaps.
- The estimates of measurement uncertainty are insufficient to account for systematic differences between measured and modelled results for gaps $\gtrsim$0.1 mm. Possible explanations are:
  - ⋆ Numerical error of FastCap calculations of capacitance. The data shown in Figure 21 would suggest that the calculated fringing capacitance is higher than that in the experiment. In the Appendix (Table 21) FastCap and FEMM calculations are compared and found to be consistent.
  - ⋆ The FastCap model is based on a simplified geometry that does not account for a number of features in the actual experiment. These include fused-silica supports that hold the high electrode in position, the specimen-entry port, and the mechanism which changes the electrode separation.
- Modelled results obtained with the mesh size parameter h_1=0.1 mm and h_1=0.2 mm agree closely. This shows that the mesh density is sufficient when $h_1 \leq 0.2$ mm.
- The marked uncertainty corridor is an estimate that represents the *change* in the actual error of FastCap calculations of capacitance between the simulations with the specimen 'in' and 'out'. While the size of the uncertainty corridor is open to some debate, its presentation on the graph is informative. As an example consider the point at t_a = 0.2 mm. The geometric capacitance is C_g=43 pF, so the ±0.2 pF uncertainty corridor at this point corresponds to an error of approximately ±0.5%. This gives an indication of the level of accuracy required of simulated capacitance values. A good (although not necessarily achievable) target for the accuracy of computations of total capacitance is 0.1% as this would enable useful corrections for a wide variety of specimens.

6 Corrections for the Effects of C_f on Lynch-Method Measurements of ϵ' for the Reentrant Cavity

6.1 TEH2 model (electrodes touch the specimen)

The symmetry considerations described in Section 3.1.1 make it possible to use program TEH2 for electrostatic calculations of the end-to-end fringing capacitance between rods that are surrounded by a hollow cylinder. A dielectric specimen can be placed between the rods. Several geometric assumptions are required:

- The rod electrodes and cylinder have infinite length, unlike the reentrant cavity (which has short-circuited ends with finite separation).
- The specimens are discs that fill the cross-section of the cylindrical shield.

- The electrodes touch the specimen with no air gap ($t_a = 0$) to fulfil the symmetry conditions.

- Electrodes and cylinder are perfectly shaped without features such as an entry port for specimens (Figure 4).

Program TEH2 should fulfil these conditions for the reentrant cavity (Figure 4) with reasonable accuracy because specimens have a larger cross-section than the electrodes, and because the length of the electrodes $\gtrsim$ diameter.

The process shown in Figure 6 for calculating the apparent permittivity by the Lynch method can also be applied to measurements in the reentrant cavity. As TEH2 is comparatively fast, the calculation of C_{out} can be performed directly, rather than by using a polynomial. Corrections to measured permittivity for fringing capacitance that are calculated with TEH2 are shown in Figure 22 and Table 11. Approximately linear variations with respect to ϵ'_{app} and t_s are observed. The correction (Y-axis) is $\approx 0.025 \times (\epsilon'_{\text{app}} - 1) \times t_s$ where t_s is given in millimetres. The effect of fringing capacitance is, according to this model, large for high-permittivity specimens even at zero gap. Actual measurements (Section 6.3) show that these corrections are overestimated.

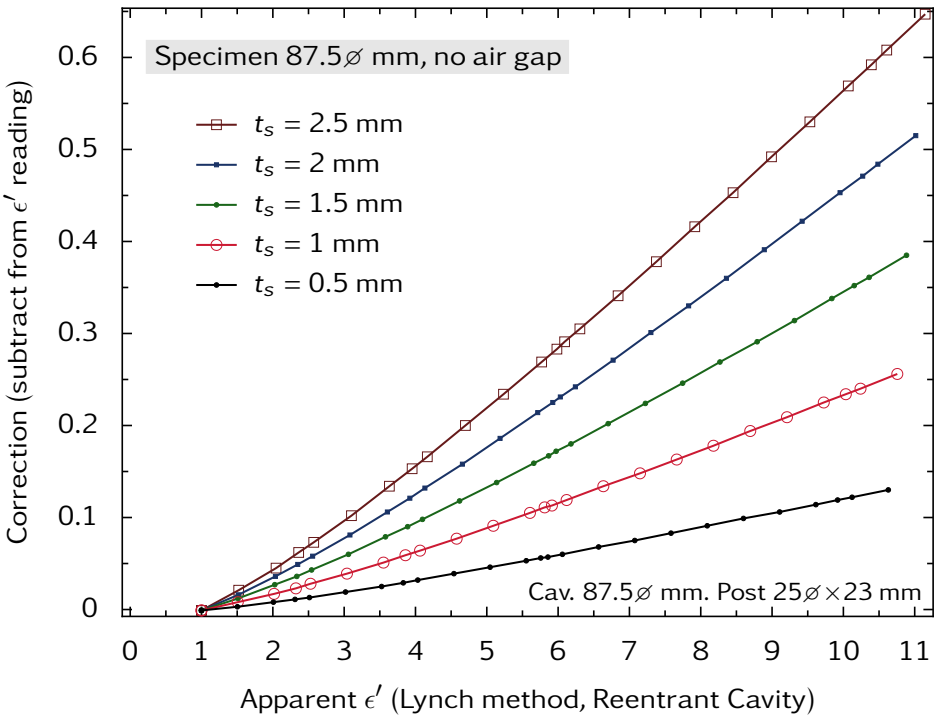

Figure 22: Permittivity corrections for measurements in the reentrant cavity for specimens of varying thickness t_s. The Y-axis shows the size of the increase in ϵ' caused by fringing capacitance. TEH2 was used for capacitance calculations of fringing capacitance. These corrections are not consistent with experiment (see Section 6.3).

Table 11: Tabulated permittivity corrections as a function of the value measured by the Lynch method (ϵ'_{app}) for the reentrant cavity (Figure 4) when there are no air gaps between specimen and electrodes ($t_a = 0$). Measurements can be corrected by subtracting the appropriate table entry. These corrections are not consistent with experiment (see Section 6.3).

Specimen thickness t_s (mm)									
0.5		1.0		1.5		2.0		2.5	
ϵ'_{app}	Corr	ϵ'_{app}	Corr	ϵ'_{app}	Corr	ϵ'_{app}	Corr	ϵ'_{app}	Corr
0.999	-0.001	0.999	-0.001	0.999	-0.001	0.999	-0.001	0.999	-0.001
1.503	0.003	1.508	0.008	1.512	0.012	1.516	0.016	1.521	0.021
2.008	0.008	2.017	0.017	2.027	0.027	2.036	0.036	2.045	0.045
2.311	0.011	2.323	0.023	2.336	0.036	2.349	0.049	2.362	0.062
2.513	0.013	2.528	0.028	2.543	0.043	2.558	0.058	2.573	0.073
3.019	0.019	3.039	0.039	3.060	0.060	3.081	0.081	3.102	0.102
3.525	0.025	3.551	0.051	3.579	0.079	3.606	0.106	3.634	0.134
3.829	0.029	3.859	0.059	3.890	0.090	3.921	0.121	3.953	0.153
4.032	0.032	4.064	0.064	4.098	0.098	4.132	0.132	4.166	0.166
4.539	0.039	4.577	0.077	4.618	0.118	4.658	0.158	4.700	0.200
5.046	0.046	5.091	0.091	5.138	0.138	5.186	0.186	5.234	0.234
5.553	0.053	5.605	0.105	5.659	0.159	5.714	0.214	5.769	0.269
5.756	0.056	5.811	0.111	5.867	0.167	5.925	0.225	5.983	0.283
5.857	0.057	5.913	0.113	5.972	0.172	6.031	0.231	6.091	0.291
6.060	0.060	6.119	0.119	6.180	0.180	6.242	0.242	6.305	0.305
6.568	0.068	6.634	0.134	6.702	0.202	6.771	0.271	6.841	0.341
7.075	0.075	7.148	0.148	7.224	0.224	7.301	0.301	7.378	0.378
7.583	0.083	7.663	0.163	7.746	0.246	7.830	0.330	7.916	0.416
8.091	0.091	8.178	0.178	8.269	0.269	8.360	0.360	8.453	0.453
8.599	0.099	8.694	0.194	8.791	0.291	8.891	0.391	8.992	0.492
9.106	0.106	9.209	0.209	9.314	0.314	9.422	0.422	9.530	0.530
9.614	0.114	9.725	0.225	9.838	0.338	9.953	0.453	10.069	0.569
9.919	0.119	10.034	0.234	10.152	0.352	10.271	0.471	10.392	0.592
10.122	0.122	10.240	0.240	10.361	0.361	10.484	0.484	10.608	0.608
10.630	0.130	10.756	0.256	10.885	0.385	11.015	0.515	11.147	0.647

6.2 FastCap models (with and without an air gap between electrodes and specimen)

The reentrant cavity is designed to accommodate rectangular specimens length 70 mm & width 54 mm that fit the entry port (Figure 4). For simulation the specimen length is reduced to 65-mm (to fit entirely within the cavity 87.5ø mm). FastCap was used to model this actual geometry. FEMM can be used for an axisymmetric geometry in which the specimen is assumed to be a disc. TEH2 can be used for a disc-shaped specimen that has the same diameter as the cavity and touches both electrodes without an air gap.

FastCap simulations, based on the symmetrical model shown in Figure 23, required approximately 100 GB of computer memory and took many hours. One stage of the process used for determining the apparent permittivity obtained by the Lynch method (Figure 6) requires the fringing capacitance of the empty cavity to be determined. Instead of using a polynomial (Table 12) fitted to FastCap results, TEH2 can be employed for this stage of the calculation (the two approaches produce almost identical results, as shown in Table 13).

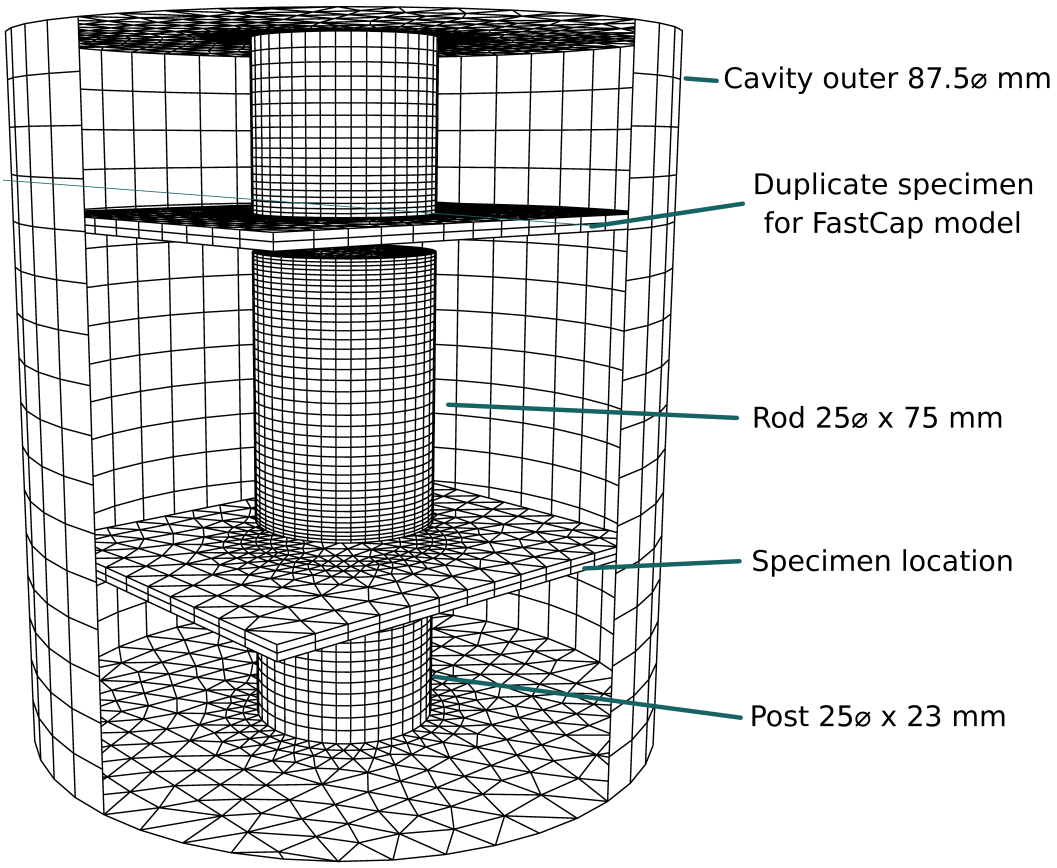

Figure 23: FastCap model of the reentrant cavity (Figure 4) for rectangular-shaped specimens. The specimens are inserted through a port in the cavity wall (omitted from the model), and sit on the post. The specimen appears twice as a symmetrical structure is used for solution.

Table 12: Polynomial coefficients of the fringing capacitance of the reentrant cavity (Figure 4) as a function of air gap between electrodes (mm). The values shown were fitted to FastCap calculations of fringing capacitance for gaps in the range 0.05 mm to 1 mm. Refer to equation (8).

Coefficient	Value
a_0	0.008 803 2
a_1	1.367 272 1
a_2	−0.859 310 7
a_3	−2.534 160 3
a_4	12.896 812 6
a_5	−22.024 277 0
a_6	16.992 447 0
a_7	−4.978 915 0

Table 13: Comparison of calculations of the fringing capacitance of the reentrant cavity (Figure 4) as a function of the air gap between the electrodes. The FastCap values were obtained from the polynomial coefficients listed in Table 12. The TEH2 values were calculated as described in Section 3.1.1. Good agreement is obtained.

Gap (mm)	C_f (mm)	
	FastCap	TEH2
0.05	1.496	1.507
0.1	1.355	1.372
0.2	1.211	1.221
0.5	1.010	1.014
1.0	0.869	0.861

6.3 Experimental results

Figure 24 shows comparisons of modelled and measured data for the reentrant cavity for the alumina specimen that was referred to in Section 5.2. The FastCap results for the contacting point (t_a=0) are calculated with a different meshing arrangement from that of the other FastCap results (as there is no intervening layer of air between top electrode and the specimen). There is insufficient data for a rigorous evaluation of uncertainty, so an estimated 'uncertainty corridor' is plotted for an uncertainty of $\Delta C = \pm 0.1$ pF where ΔC is the uncertainty of the change in the calculated fringing capacitance between 'in' and 'out' measurements. The value $\Delta C = \pm 0.1$ pF is obtained from the difference between FastCap and TEH2 values at zero gap (also plotted). C_f/C_g of the reentrant cavity is approximately twice that of the Hartshorn and Ward electrode-system because the electrode circumference/area ratio is double [5].

The measurements on alumina obtained by using the Lynch method (Equation 1) without any correction for fringing capacitance (Figure 24) are, to within experimental uncertainty, consistent with the reference value for $t_a \leq 0.1$ mm. The values of apparent permittivity forecast from computations of C_f with FastCap are outliers in comparison to the experimental data, although TEH2 and FastCap values at $t_a = 0$ agree to within 0.1 pF. This seems to indicate that the calculations of C_f are valid, but the electrostatic model is not an accurate description of the fringing capacitance and a high-frequency analysis that considers the resonant mode is needed.

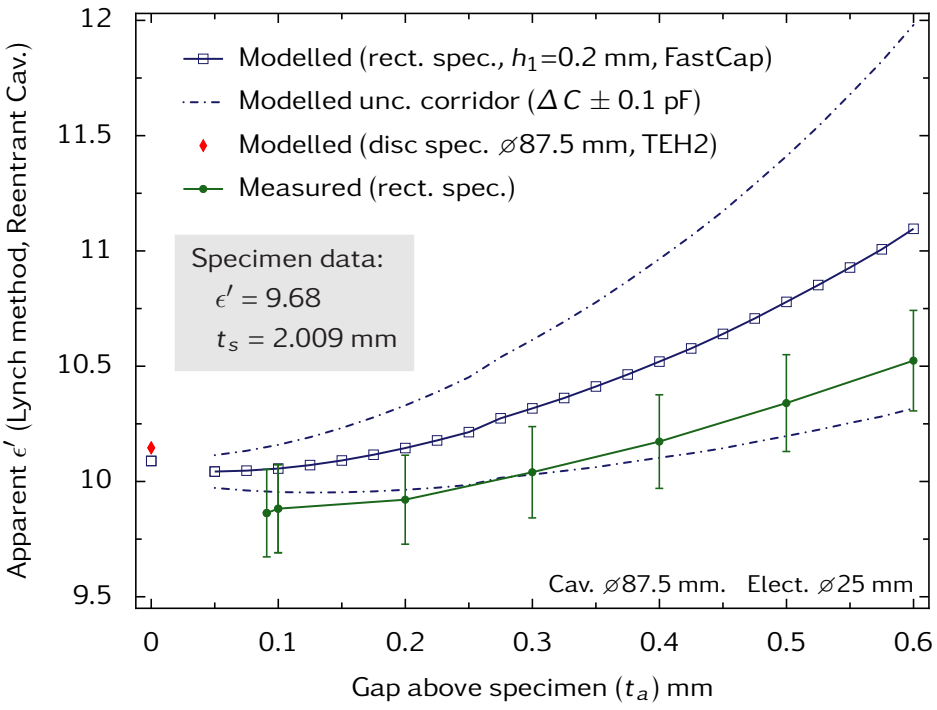

Figure 24: Measurements of ϵ' by the Lynch method as a function of the air gap above the specimen made with the reentrant cavity at 300 MHz. Modelled values are also shown. The observed dependence of ϵ' on t_a is a consequence of fringing capacitance, for which no corrections are applied. The specimen was a rectangle of alumina, dimensions 75×54×2.009 mm. The uncertainties of the experimental data are shown for a coverage factor of $k = 2$. These are obtained from estimates of the uncertainty associated with the specimen thickness and the micrometer readings.

7 Analysis and Conclusion

- Comprehensive comparisons of fringing capacitance (C_f) calculations have been made with software that uses mode-matching, and three types of discretised model (Section 4). Where available, published data, and data for calculable geometries were also included in the comparison. For fully-shielded geometries, such as coaxial capacitors, close agreement was obtained except in a few cases when geometries with small inter-electrode gaps were studied. For a capacitor with unshielded disc-shaped electrodes, C_f obtained with software that uses discretised models showed significant discrepancies. The Kirchhoff formula gave the lowest values of C_f.

- Mode-matching programs TEH2 and TICELL provide rapid and accurate computation of C_f for a limited range of coaxial geometries. These programs do not require discretisation of surfaces or the space between them. For best accuracy at least 128 modes are needed, but even so computations take a second or less.

- The settings and meshing used for calculations of C_f that use discretised models can have a critical effect because it is obtained by subtracting two comparatively-large numbers: the total capacitance and the geometric capacitance.

- A comparison of calculations of C_f for a coaxial geometry (Table 5) shows exact agreement between TEH2 and FEMM (2D discretisation) to three significant figures, even when the inter-electrode gap is small. With a computer with 32 GB of memory, this level of agreement was not achievable with programs FastCap (surface discretisation) or NGSolve (3D discretisation) for the full range of gaps. FEMM was found to be fast, straightforward to use, and accurate.

- FastCap and FEMM calculations of C_f for the electrode system used in Hartshorn and Ward apparatus were found to be in good agreement (Section B.3.1). This substantiates the accuracy of fringing capacitance corrections obtained by using FastCap in earlier work [17].

- Further comparisons of C_f calculated with TEH2 and FastCap have been carried out (Appendix B.1 and B.2) for coaxial capacitors of various geometries. When the conductors are air-spaced, close agreement is obtained (Tables 13, 14 and 18). The introduction of a disc of dielectric material results in discrepancies that increase with permittivity (Tables 16 and 17). For $\epsilon' = 10$ the largest discrepancy is 6 %.

- The measurement of permittivity and loss angle of sheets of material in parallel-electrode systems by the Lynch (equivalent-thickness) method has been described (Section 2.4). If unguarded electrodes are used, and specimens have larger area than the electrodes, the measured (apparent) permittivity is found to be greater than the actual permittivity as a result of C_f. The error increases with the size of the air gap between specimen and top electrode for the 'in' measurement, but even when the air gap is zero there is an error. These experimental findings are consistent with predictions based on modelling. Such errors can be corrected for if C_f can be calculated for 'in' and 'out' measurements (Figure 6).

- For the Hartshorn and Ward apparatus, measurements of permittivity obtained with the Lynch method have been shown to have improved accuracy if corrections for fringing capacitance are applied. Measurements on several materials are given in reference [17].

- For the 300 MHz reentrant cavity, measurements of permittivity obtained for an alumina specimen by the Lynch method without corrections for the effects of C_f are consistent with the reference value when the air gap is small ($t_a \lesssim 0.1$ mm). In other words, fringing capacitance between the electrodes has little effect on the measured permittivity. This is contrary to predictions obtained by using TEH2 and FastCap software to model fringing capacitance. This may be because the energy distribution of a high-frequency resonant mode is not accounted for in an electrostatic analysis.

- TEH2 software, long available at NPL, can be used for rapid corrections for the effects of C_f on permittivity measurements in low-frequency coaxial systems when the electrodes are long rods (length $\gtrsim$ diameter) and the air gap between electrodes and specimens is minimal. Experimental data presented shows that a small air gap between the specimen and the top electrode (e.g. 0.1 mm for 50 mm⌀ electrodes) does not have a significant effect on the size of the correction for measurements by the Lynch method for $\epsilon' \lesssim 10$. The disc-shaped electrodes of the Hartshorn and Ward apparatus currently used at NPL are too short to enable accurate corrections to be obtained with TEH2 (see Table 8) – an aspect that should be considered in any future re-design.

- For measurement of permittivity in the Hartshorn and Ward apparatus when specimens have a smaller area than the electrodes (i.e. they do not impinge on the fringing fields) [16] it is only necessary to consider the C_f of air-spaced electrodes, which has been calculated precisely with FEMM and FastCap. The calculation process shown in Figure 6 can easily be amended for small-area specimens. It is expected that the uncertainty of measurements of the permittivity of high-permittivity materials ($\epsilon' \gtrsim 10$) can be reduced by this approach.

- A further application for calculations of the C_f of air-spaced electrodes arises in measurements of dielectric *loss angle* in Hartshorn and Ward apparatus: Parallel and stray capacitance in these systems causes some of the resonant current to bypass the resonator causing apparent loss in the system to be "diluted". Corrections for the effects of dilution can, as a result of this work, be calculated with improved accuracy [17].

- This report has some relevance to *bridging the LF–RF gap*; an important topic in impedance metrology. The "gap" refers to frequencies that are too high for four-terminal methods but not ideal for VNA methods because calibration kits provide only partial traceability. It is typically understood to include the range 3 MHz to 300 MHz (HF & VHF), although interpretations vary. The recent publications by Agustoni & Overney [41] and by Shilov et al. [42] respectively consider calculable parallel-plate and coaxial capacitors designed for use in the LF–RF gap. The COMSOL model used by Agustoni & Overney is notable because the skin effect is accounted for, and is found to have an observable effect at frequencies above 40 MHz.

8 Acknowledgements

Support from Sonnet Software Inc., COMSOL Ltd, and the NGSolve mailing list is acknowledged.

A Technical Details of how to use the FastCap Program

A.1 Compilation

FastCap can be downloaded as C source code[8]. It is assumed that the Whiteley Research version will be used. The GNU Compiler Collection (GCC) C compiler can be used to compile FastCap after unzipping the downloaded files to a convenient directory. Prior to compiling edit the Makefile in the FastCap source directory to ensure the compilation flags are set appropriately. To compile with optimisation for maximum speed use CFLAGS = -DOTHER -Ofast. This gives a five-fold improvement in execution time compared to code compiled without optimisation (options CFLAGS = -DOTHER -O0). Execution-time checks for e.g. numeric overflow are disabled by the -Ofast option, but it was found that using the optimiser did not change computed results. To compile and link FastCap on Linux, open a terminal, change the directory to the location of FastCap, and type ./config followed by make fastcap. On Windows install MSYS2[9], then install the 64-bit GCC C compiler from within MSYS2 and follow exactly the same steps as for Linux.

A.2 Mesh generation with netgen

Additional software is required to generate mesh files [43], as FastCap does not have a built-in mesh generator. Only surface meshes are required. For the work described in this report *netgen* [44] (included in NGSolve v6.2) was used. This has a Python interface, which allows the process of generating meshes to be automated. End faces were meshed with triangular elements by using netgen – see Figure 25 and Code Listing 1. Meshes for all of the circular faces (central disc or rod, cylindrical shield, and dielectric disc if present) are generated in one step by creating a 2D circular mesh that includes annular boundaries. The size of the finest mesh (which is at an annular boundary that corresponds to the periphery of the inner electrode) is defined by h_1 (units: mm). Appendix B.1 describes how the mesh densities of different regions were chosen. Netgen meshes were saved as text files (with file extension .vol). These files include the integer boundary conditions specified by bc in the Python script, which enables the files to be parsed to extract the meshes for each region and edge of the circular face. Vertices in the mesh are specified by integer indexes, which refer to row numbers of a block of (x, y, z) coordinate data

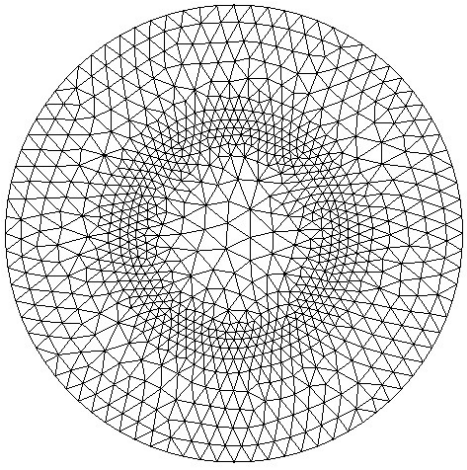

Figure 25: Annular face with varying mesh density created with *netgen*.

[8] http://www.wrcad.com/freestuff.html
[9] https://www.msys2.org/

Listing 1: A Python function for meshing a circular face that has increased mesh density at an internal boundary, as shown in Figure 25. This corresponds to the edge of a nearby disc or rod electrode. The mesh is saved to a text file.

```
from netgen.geom2d import SplineGeometry

def MeshAnnulus(inner_radius, outer_radius, h1, h3, h4,
    fn="annular_face.vol"):
    """
        Create mesh of face of annulus, and also the central
        region inside annulus.
        Mesh data can be extracted from the output file later.
        h1 is mesh size at annular boundary
        h3 is mesh size around outer edge
        h4 is mesh size at centre of annulus (None to use default)
        h1 < h3 < h4
    """
    assert inner_radius < outer_radius
    geo = SplineGeometry()
    geo.AddCircle(c=(0,0), r=outer_radius, bc=2,
                  leftdomain=1, rightdomain=0, maxh=h3)
    geo.AddCircle(c=(0,0), r=inner_radius, bc=4,
                  leftdomain=2, rightdomain=1, maxh=h1)
    if h4 is None:
        ngmesh = geo.GenerateMesh()
    else:
        ngmesh = geo.GenerateMesh(maxh=h4)
    ngmesh.Save(fn)
```

at the end of the file. Side faces were meshed with rectangular elements that were generated by using 'for loops'. Full 3D surface meshes that are continuous at corners and contacting boundaries could therefore be obtained. The coordinates of the vertices of the mesh elements were saved as text files. The format of files of triangular meshes (used for circular faces) that is required by FastCap is shown in Listing 2. Files of rectangular meshes (used for side walls) are similar except that data rows begin with Q and contain twelve numbers (the coordinates of the four vertices of each element). Each row includes a label (TDiel for this file), which can be chosen arbitrarily.

Listing 2: Example text file containing triangular meshes (lines of nine numbers are truncated).

```
0 top_diel
T TDiel  0.000000000000 -48.000000000000 37.500000000000  ...
T TDiel  5.795194875404 -47.648879486889 37.500000000000  ...
etc.
```

A.3 Using FastCap from batch files

FastCap can be run from the command line (or from within Python by using the subprocess module). The FastCap download includes a manual [45] which gives a full description of the command line options. For the work reported the command line used was

```
fastcap -lcap.lst -o4 -t0.001  .
```

Options -o4 and -t0.001 specify that calculations are to be made with high accuracy. Option -t0.001 specifies the exit condition of an iterative loop: namely the capacitance solution changing by 0.1% or less. Setting option -t to a smaller value did not change the computed results. Option -l specifies that a batch file cap.lst is to be used. This file must be prepared carefully. After the calculation is completed, FastCap writes the Maxwell capacitance matrix of elements $m_{i,k}$ to the terminal console (or into a string if using the check_output function of the Python subprocess module). For two electrode systems a 2×2 matrix is calculated. The required inter-electrode capacitance is $(-1) \times m_{1,2}$ or $(-1) \times m_{2,1}$ (which should have the same value).

Listing 3 is the batch file used for determining the total capacitance of the geometry shown in Figure 30. This example assumes that the dielectric disc is polythene, ϵ'=2.3. As FastCap expects SI units, if dimensions are given in mm (as is the case here), the output Maxwell capacitance matrix can be converted to Farads by multiplying by 0.001.

Each electrode or dielectric is preceded by a line beginning G (indicating a group). Conductors are defined by lines of the form

C file_name $\boxed{\epsilon'}_{\text{outside}}$ Xoff Yoff Zoff [+]

where Xoff, Yoff and Zoff are coordinates offsets (set to zero if not needed), and the optional + is used to indicates that files are appended. For the high electrode, three files must be used as the permittivity against the side wall (1.0006, air) is different to that against the end faces (2.3, polythene).

Dielectrics are defined by lines of the form:

D file_name $\boxed{\epsilon'}_{\text{outside}}$ $\boxed{\epsilon'}_{\text{inside}}$ Xoff Yoff Zoff Xpt Ypt Zpt –

where Xpt, Ypt and Zpt are the absolute coordinates of a point inside the dielectric. Contact areas with metal electrodes are not meshed (see Figure 26).

Listing 3: FastCap batch file cap.lst for the geometry shown in Figure 30.

```
G High_Electrode
C high.txt 1.0006    0.0  0.0  0.0 +
C high_dtop.txt 2.3  0.0  0.0  0.0 +
C high_dlwr.txt 2.3  0.0  0.0  0.0
*
G Top_Diel
D top_diel.txt 1.0006 2.3 0.0 0.0 0.0   0.0 0.0 38.5 -
*
G Lwr_Diel
D lwr_diel.txt 1.0006 2.3 0.0 0.0 0.0  0.0 0.0 -38.5 -
*
G Shield
C shield.txt 1.0006   0.0  0.0  0.0
```

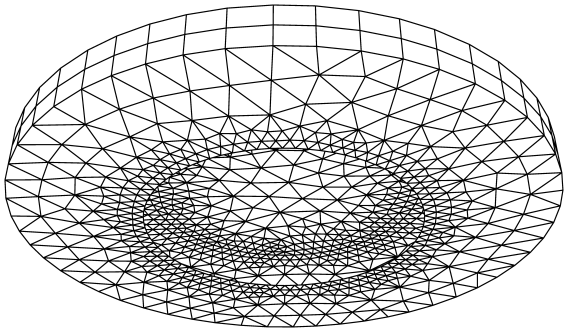

Figure 26: Mesh for the top dielectric disc in Figure 30. The unmeshed area is placed against the meshed end of the rod electrode.

B Supplementary Results

This section contains calculations of the fringing capacitance of a rod or disc-shaped electrode surrounded by a cylinder that is closed at one end. A variation in which the closed end is reentrant is also considered. For some of these calculations, a disc or rectangle of dielectric material is placed between the electrodes. The tests made were chosen with the following main objectives:

- To show that FastCap and FEMM calculations of fringing capacitance for the Hartshorn and Ward apparatus (Section 2.3.1) are consistent. This is to support findings given in reference [17].
- To show that the TEH2 and FastCap calculations of fringing capacitance for the reentrant cavity (Section 2.3.2 and 3.1.1) are consistent.
- Study the effect of varying the mesh size parameter h_1 (Section 3.2) for FastCap. When there are gaps that are small in relation to other dimensions it is desirable to use a low value of h_1 to obtain high accuracy. In practice, compromises often have to be made because of high memory-usage and long computational times.

FEMM requires only 2D meshing so is comparatively rapid and efficient in it's use of memory. In every case the mesh size could be reduced until it no longer had any significant bearing on results. FEMM cannot be used when the dielectric material is rectangular as it supports only axisymmetric geometries.

B.1 Long rod-shaped electrode surrounded by a cylinder

Test results are presented for cases in which the space between the end of the rod electrode and the end of the cylinder is filled by (i) air, (ii) a dielectric disc and (iii) a dielectric disc and a thin layer of air.

For all results, the conductor diameters were 108 mm (cylinder) and 50 mm (inner conductor rod). FastCap results were computed with inner-conductor rods that are 1.5 diameters (75 mm) long, which is sufficient to ensure that the fringing capacitance is not affected significantly by interactions between the fields at the truncated ends.

In the results shown in Appendix B.1 and B.2, C_{end} refers to the capacitance between the discontinuity plane marked in Figure 7, and the short-circuited end of the surrounding cylinder. C_f is obtained by subtracting the geometric end capacitance, C_g.

B.1.1 As a function of the end air-gap

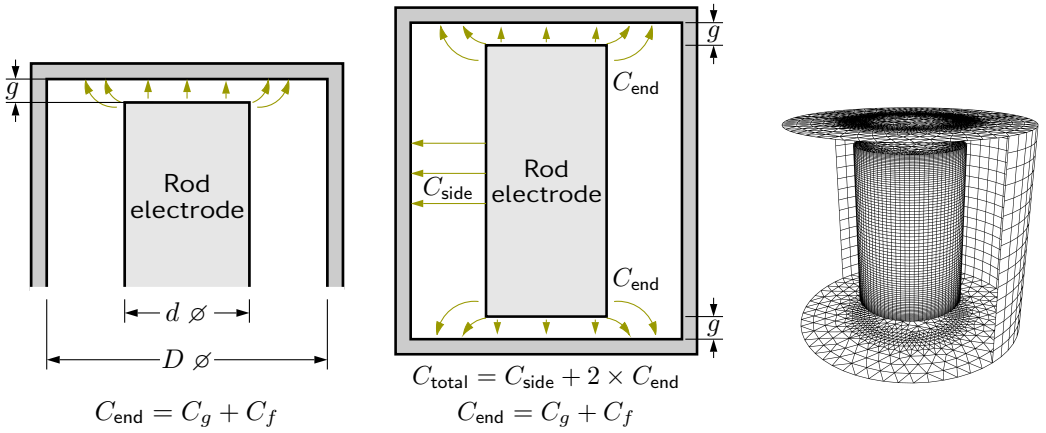

(a): TEH2 calculation **(b):** FastCap calculation **(c):** Mesh

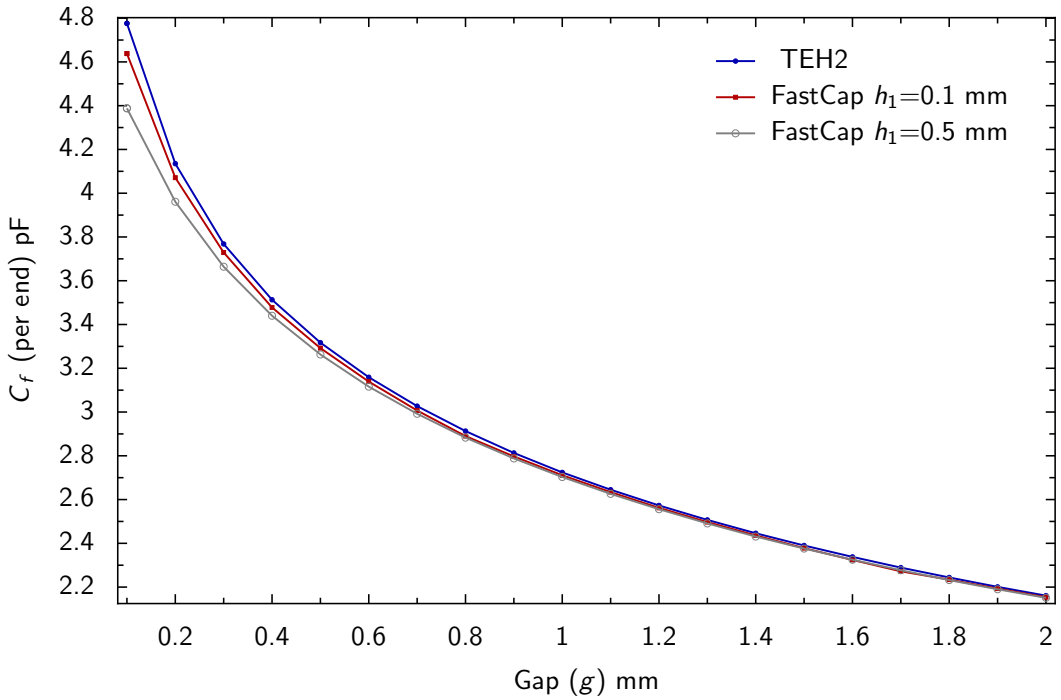

(d): Comparison of fringing capacitance at one end of rod electrode calculated with TEH2 and FastCap.

Figure 27: Comparison of C_f calculated with TEH2 as function of g (assumes infinitely-long rod electrode and surrounding cylinder) and FastCap (rod electrode length 75 mm, same gap at each end). The diameters of the cylinder and the rod electrode were 108 mm and 50 mm respectively. FastCap calculations with the mesh-size parameter h_1 set to 0.1 mm and 0.5 mm are shown. The data shown is tabulated in Table 14.

Table 14: Tabulated values of fringing capacitance at one end of rod electrode obtained by using FastCap and TEH2 for the geometry shown in Figure 27 for a range gaps.

Gap (mm)	C_f (pF)				
	FastCap h_1=0.1 mm	FastCap h_1=0.2 mm	FastCap h_1=0.5 mm	FastCap h_1=1 mm	TEH2
0.1	4.638	4.598	4.388	4.048	4.777
0.2	4.071	4.046	3.961	3.766	4.135
0.3	3.729	3.714	3.664	3.539	3.768
0.4	3.478	3.477	3.440	3.353	3.513
0.5	3.292	3.292	3.263	3.197	3.317
0.6	3.139	3.140	3.116	3.064	3.159
0.7	3.007	3.009	2.992	2.949	3.027
0.8	2.890	2.895	2.883	2.846	2.913
0.9	2.797	2.798	2.788	2.756	2.813
1.0	2.711	2.712	2.703	2.674	2.724
1.1	2.634	2.634	2.626	2.601	2.645
1.2	2.562	2.563	2.556	2.533	2.573
1.3	2.497	2.497	2.491	2.471	2.507
1.4	2.436	2.436	2.431	2.413	2.446
1.5	2.378	2.380	2.376	2.360	2.390
1.6	2.324	2.327	2.325	2.310	2.338
1.7	2.272	2.276	2.277	2.264	2.289
1.8	2.234	2.236	2.232	2.220	2.244
1.9	2.193	2.194	2.190	2.178	2.201
2.0	2.154	2.154	2.151	2.140	2.161

B.1.2 As a function of the length of the rod electrode

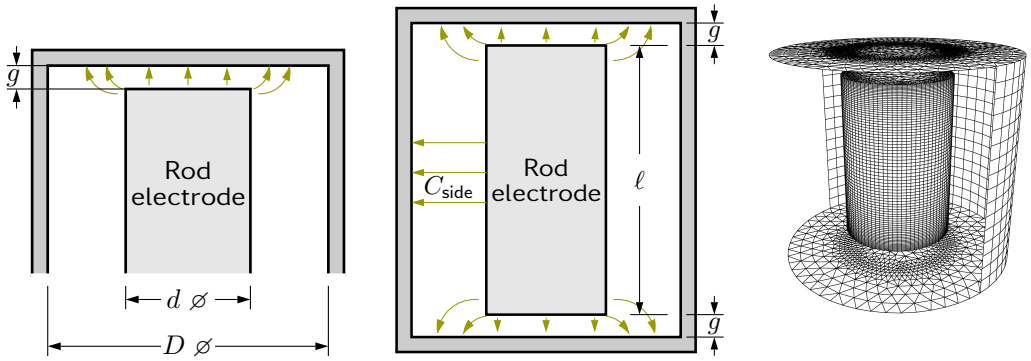

(a): TEH2 calculation **(b):** FastCap & FEMM calculation **(c):** Mesh

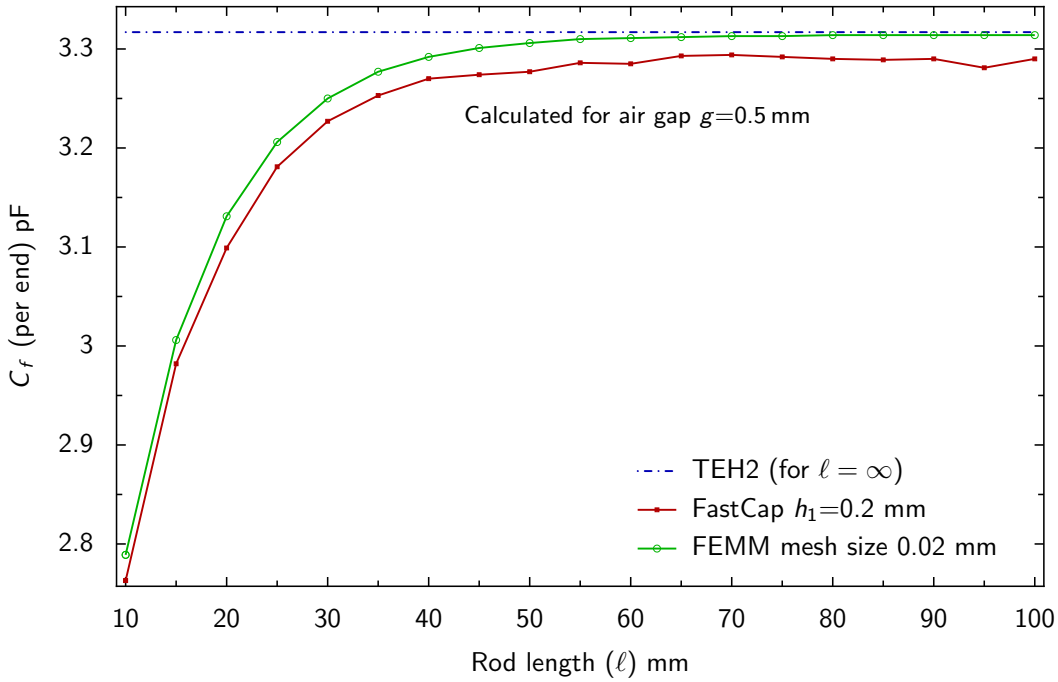

(d): Comparison of fringing capacitance at one end of rod electrode calculated with TEH2, FEMM and FastCap

Figure 28: Comparison of C_f calculated with TEH2 and FastCap as function of rod length, ℓ. The TEH2 calculations assume that the rod electrode and surrounding cylinder are infinitely-long. FastCap calculations were made with the same gap (0.5 mm) at each end, and the the mesh-size parameter h_1 set to 0.2 mm. The diameters of the cylinder and the rod electrode were 108 mm and 50 mm respectively. The data shown is tabulated in Table 15.

Table 15: Tabulated values of fringing capacitance at one end of rod electrode obtained by using FastCap and FEMM for the geometry shown in Figure 28 for a range of lengths of central rod. The gap g was 0.5 mm. The data is plotted in Figure 28. The mesh-size parameter h_1 for the FastCap calculations was 0.2 mm. The mesh size in the high-field region was 0.02 mm for the FEMM calculations. For this geometry, TEH2 gives C_f=3.317 pF for $\ell = \infty$.

ℓ (mm)	C_f (pF)	
	FastCap h_1=0.2 mm	FEMM
10	2.763	2.789
15	2.982	3.006
20	3.099	3.131
25	3.181	3.206
30	3.227	3.250
35	3.253	3.277
40	3.270	3.292
45	3.274	3.301
50	3.277	3.306
55	3.286	3.310
60	3.285	3.311
65	3.293	3.312
70	3.294	3.313
75	3.292	3.313
80	3.290	3.314
85	3.289	3.314
90	3.290	3.314
95	3.281	3.314
100	3.290	3.314

B.1.3 With dielectric disc, as a function of ϵ'

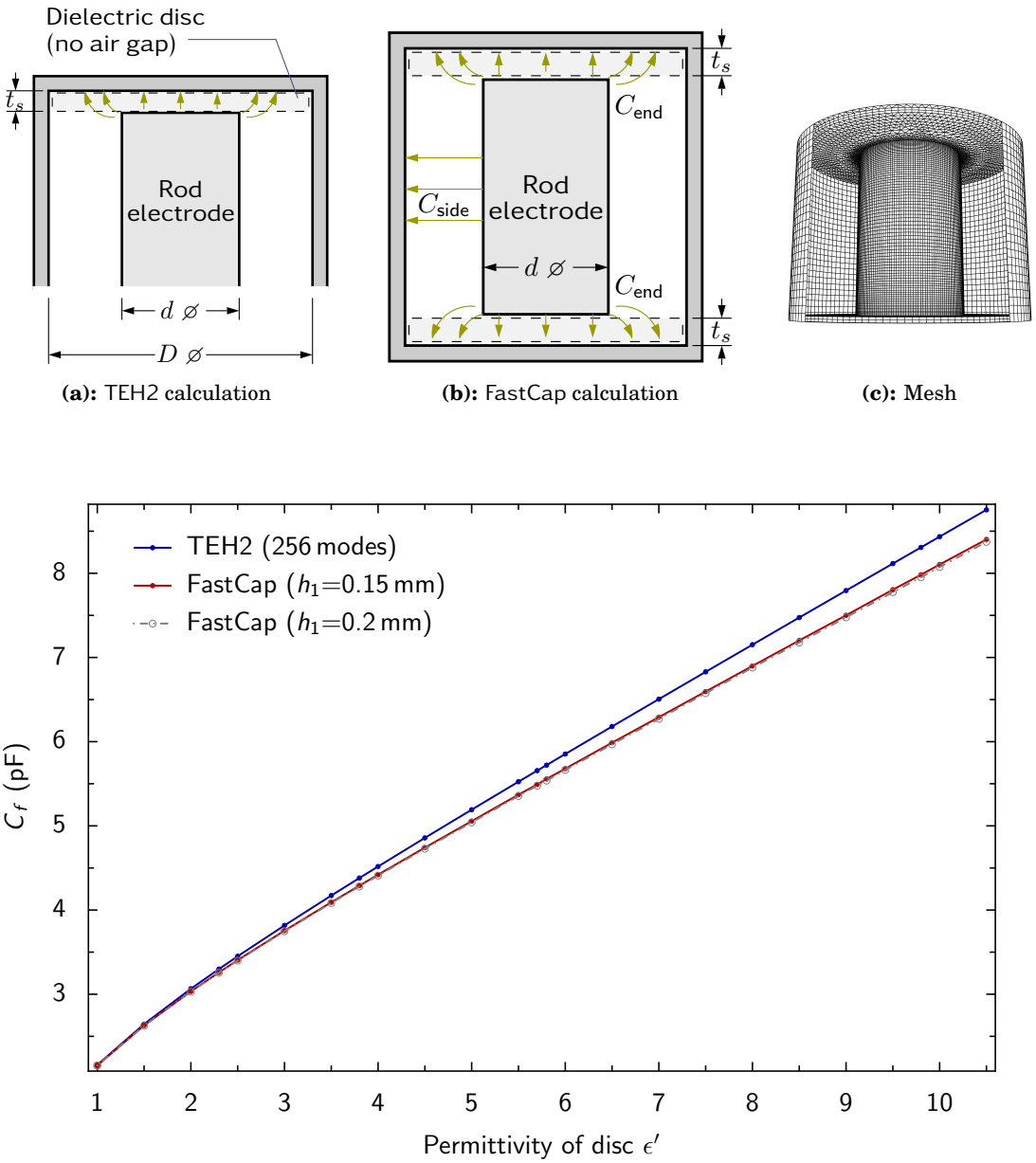

(a): TEH2 calculation **(b):** FastCap calculation **(c):** Mesh

(d): Calculated fringing capacitance at one end of rod electrode.

Figure 29: Comparison of C_f calculated with TEH2 and FastCap between a rod electrode and surrounding cylinder with dielectric disc 2 mm thick. The diameters of the cylinder and the rod electrode were 108 mm and 50 mm respectively. For the FastCap calculation, the rod electrode length is 75 mm, and the geometry is made symmetrical by including a duplicate dielectric disc. The data shown is tabulated in Table 16.

Table 16: Tabulated values of fringing capacitance at one end of rod electrode with dielectric disc obtained by using FastCap FEMM and TEH2 for the geometry shown in Figure 29 for a range of permittivity (ϵ'). At ϵ'=10, TEH2 and FastCap values differ by 4%.

ϵ'	C_f (pF)			
	FastCap h_1=0.15	FastCap h_1=0.2	FEMM‡	TEH2
1.0	2.154	2.153	2.162	2.160
1.5	2.629	2.626	2.647	2.645
2.0	3.034	3.030	3.066	3.065
2.3	3.259	3.255	3.301	3.299
2.5	3.405	3.399	3.453	3.451
3.0	3.755	3.748	3.819	3.817
3.5	4.092	4.083	4.173	4.172
3.8	4.289	4.280	4.382	4.380
4.0	4.420	4.409	4.519	4.517
4.5	4.741	4.728	4.859	4.857
5.0	5.056	5.041	5.194	5.192
5.5	5.370	5.355	5.526	5.524
5.7	5.492	5.477	5.658	5.656
5.8	5.557	5.537	5.724	5.721
6.0	5.679	5.664	5.855	5.853
6.5	5.988	5.968	6.183	6.180
7.0	6.291	6.271	6.508	6.505
7.5	6.595	6.575	6.832	6.829
8.0	6.899	6.879	7.155	7.152
8.5	7.202	7.177	7.477	7.474
9.0	7.501	7.476	7.799	7.795
9.5	7.805	7.775	8.119	8.115
9.8	7.982	7.952	8.311	8.307
10.0	8.104	8.074	8.439	8.435
10.5	8.402	8.372	8.759	8.754

‡FEMM mesh size 0.02 mm in the vicinity of the electrodes, and 'Auto' elsewhere.

B.1.4 With air gap and dielectric disc, as a function of ϵ'

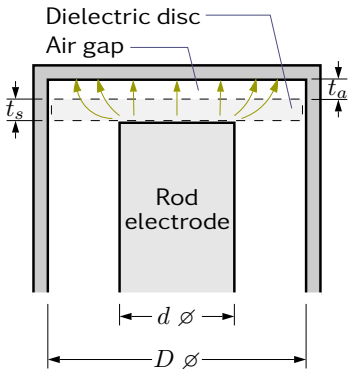

(a): TEH2 calculation

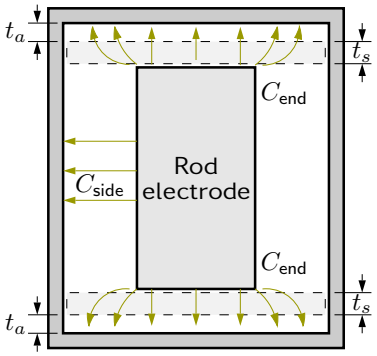

(b): FastCap calculation

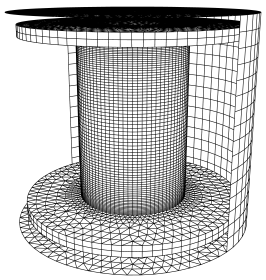

(c): Mesh

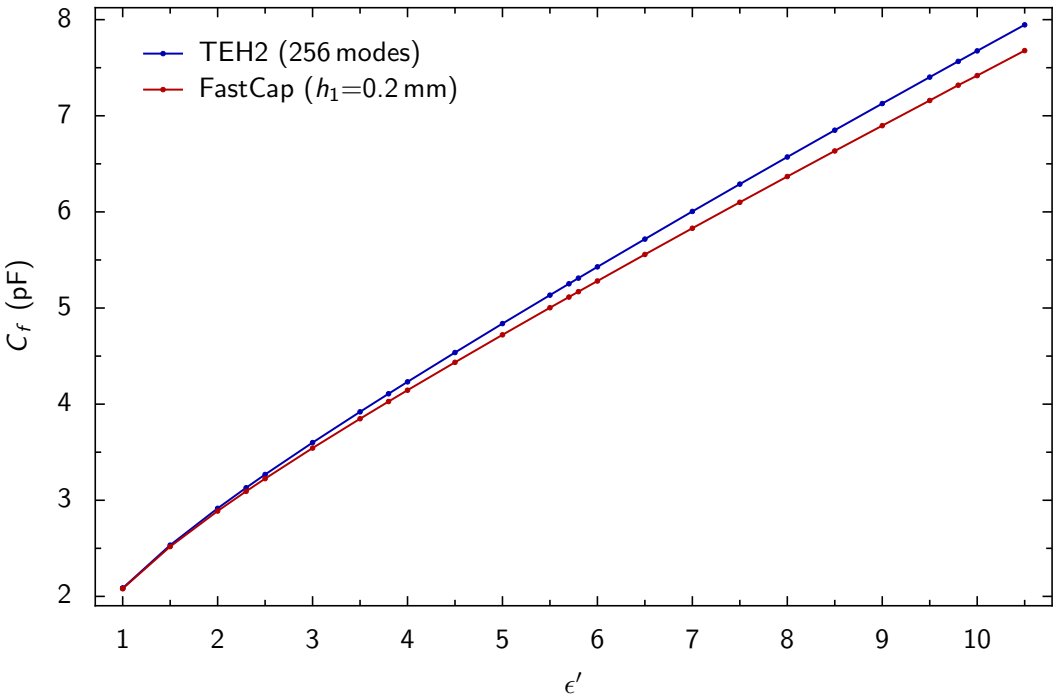

(d): Calculated fringing capacitance at one end of rod electrode

Figure 30: Comparison of C_f calculated with TEH2 and FastCap between a rod electrode and surrounding cylinder with dielectric disc 2 mm thick and a 0.2 mm air gap. TEH2 assumes that the rod electrode and cylinder have infinite length. The diameters of the cylinder and the rod electrode were 108 mm and 50 mm respectively. For the FastCap calculation, the rod electrode length is 75 mm, and the geometry is made symmetrical by including a duplicate dielectric disc/air gap. The data shown is tabulated in Table 17.

Table 17: Tabulated values of fringing capacitance at one end of rod electrode with dielectric disc obtained by using FastCap, FEMM and TEH2 for the geometry shown in Figure 30 for a range of permittivity (ϵ') values. At ϵ'=10, TEH2 and FastCap values differ by 3.5%.

ϵ'	C_f (pF)		
	FastCap h_1=0.2	FEMM‡	TEH2
1.0	2.081	2.087	2.086
1.5	2.518	2.535	2.533
2.0	2.888	2.918	2.916
2.3	3.093	3.132	3.130
2.5	3.225	3.270	3.268
3.0	3.543	3.602	3.600
3.5	3.848	3.923	3.920
3.8	4.027	4.111	4.108
4.0	4.145	4.235	4.232
4.5	4.435	4.541	4.537
5.0	4.721	4.841	4.838
5.5	5.003	5.138	5.134
5.7	5.114	5.256	5.252
5.8	5.170	5.315	5.311
6.0	5.281	5.432	5.428
6.5	5.557	5.722	5.717
7.0	5.830	6.009	6.005
7.5	6.100	6.294	6.289
8.0	6.368	6.576	6.571
8.5	6.634	6.856	6.850
9.0	6.897	7.133	7.127
9.5	7.159	7.408	7.402
9.8	7.318	7.572	7.566
10.0	7.418	7.681	7.675
10.5	7.678	7.952	7.946

‡FEMM mesh size 0.02 mm in the vicinity of the electrodes, and 'Auto' elsewhere.

B.2 Long rod-shaped electrode surrounded by a reentrant cylinder

Symmetry considerations enable TEH2 to be used to calculate the capacitance between two infinitely-long rods inside a reentrant cylinder – see Section 3.1.1. For an alternative implementation, see [46]. The results presented in this section establish that FastCap calculations for a "long" rod electrode (length 3 radii) give comparable results to TEH2. Calculations made with FEMM and FastCap are compared in Section B.3.

B.2.1 As a function of the end air-gap

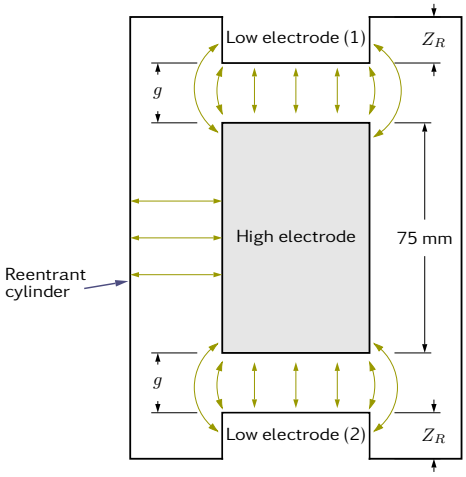

(a): FastCap calculation

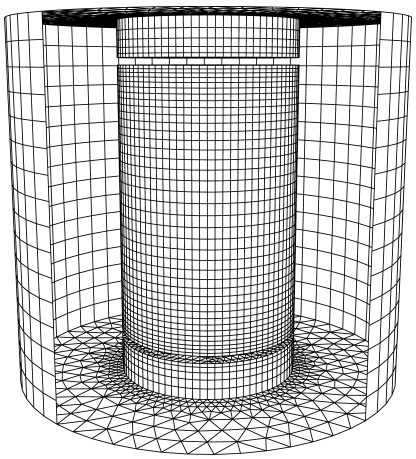

(b): Mesh

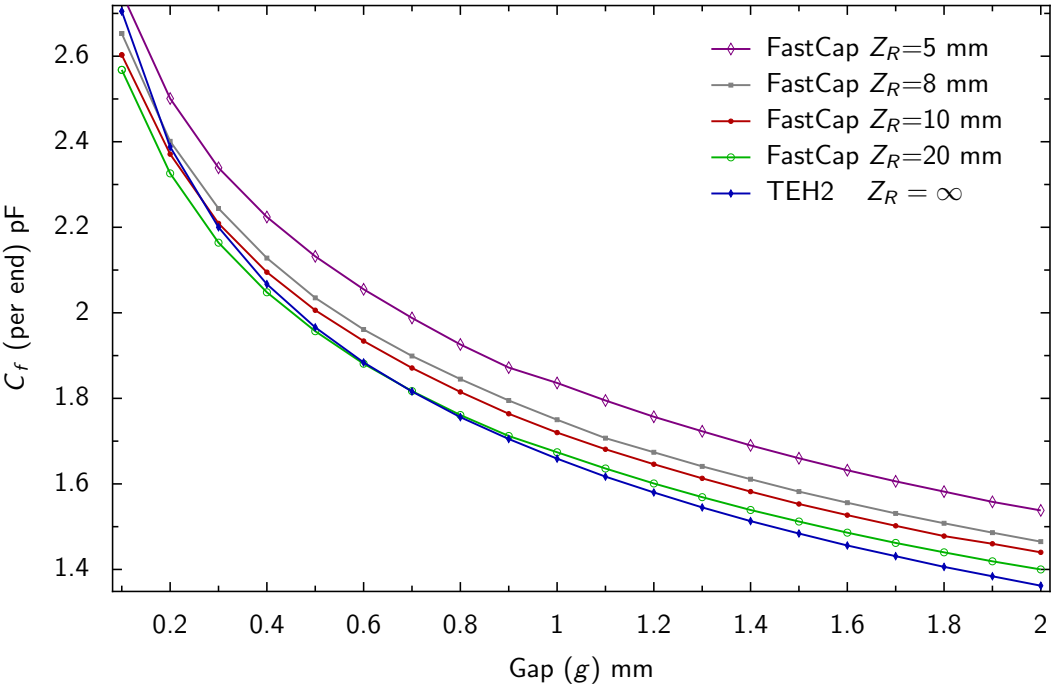

(c): Comparison of fringing capacitance calculated with TEH2 and FastCap.

Figure 31: Comparison of C_f calculated with TEH2 and FastCap as a function of gap (g). The conductor diameters were 108 mm (reentrant cylinder) and 50 mm (inner). FastCap results were obtained for rod electrode length 75 mm and a few values of the offset length, Z_R. The mesh-size parameter h_1 was 0.2 mm. The data shown is tabulated in Table 18.

Table 18: Tabulated values of fringing capacitance obtained by using FastCap and TEH2 for the geometry shown in Figure 31 for a range gaps. FastCap results were obtained for a few values of the offset length, Z_R (marked in Figure 31a). The mesh-size parameter h_1 for the FastCap calculations was 0.2 mm.

	C_f (pF)				
Gap g (mm)	FastCap Z_R=5 mm	FastCap Z_R=8 mm	FastCap Z_R=10 mm	FastCap Z_R=20 mm	TEH2
0.1	2.748	2.653	2.603	2.568	2.705
0.2	2.501	2.401	2.371	2.326	2.388
0.3	2.339	2.244	2.209	2.164	2.200
0.4	2.224	2.128	2.095	2.048	2.067
0.5	2.132	2.035	2.006	1.957	1.966
0.6	2.055	1.961	1.934	1.881	1.884
0.7	1.988	1.899	1.871	1.817	1.816
0.8	1.926	1.845	1.815	1.761	1.756
0.9	1.872	1.795	1.764	1.712	1.705
1.0	1.836	1.750	1.720	1.674	1.659
1.1	1.795	1.707	1.681	1.636	1.617
1.2	1.757	1.674	1.646	1.601	1.580
1.3	1.723	1.641	1.613	1.569	1.545
1.4	1.690	1.611	1.582	1.539	1.513
1.5	1.660	1.582	1.553	1.512	1.484
1.6	1.632	1.556	1.527	1.486	1.456
1.7	1.606	1.531	1.502	1.462	1.431
1.8	1.582	1.508	1.478	1.440	1.406
1.9	1.558	1.486	1.460	1.419	1.384
2.0	1.538	1.465	1.440	1.400	1.362

B.2.2 As a function of the diameter of the reentrant cylinder

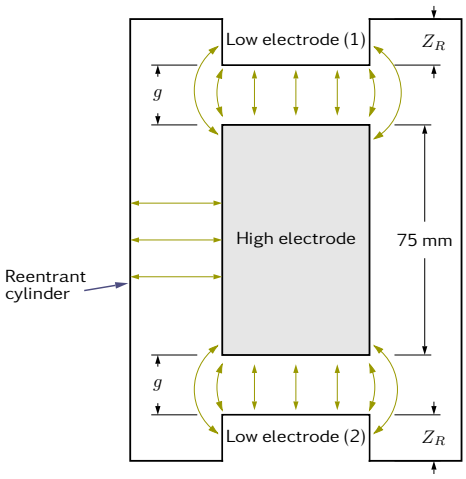

(a): FastCap calculation

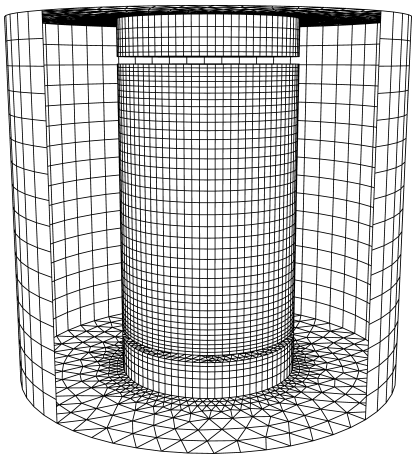

(b): Mesh

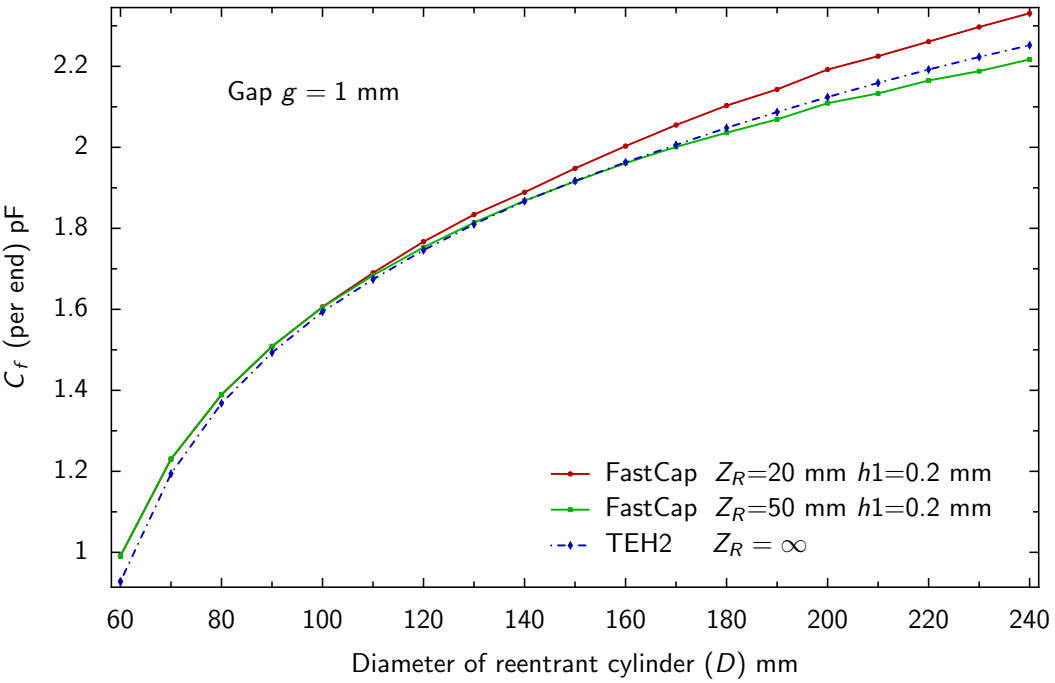

(c): Comparison of fringing capacitance calculated with TEH2 and FastCap as a function of the diameter of the reentrant cylinder.

Figure 32: Comparison of C_f calculated with TEH2 and FastCap as a function of the diameter of the reentrant cylinder (D). The inner conductor diameter was 50 mm and the gap g between the reentrant cylinder and the rod electrode at each end was 1 mm. FastCap results were obtained for rod electrode length 75 mm and offset lengths Z_R of 20 mm and 50 mm. The mesh-size parameter h_1 was 0.2 mm. The data shown is tabulated in Table 19.

Table 19: Tabulated values of fringing capacitance obtained by using FastCap and TEH2 for the geometry shown in Figure 32 for a range of diameters of the reentrant cylinder. FastCap results were obtained for two values of the offset length, Z_R (marked in Figure 32b).

$D\varnothing$ (mm)	C_f (pF)			
	FastCap Z_R=20 mm h=0.2 mm	FastCap Z_R=20 mm h=0.15 mm	FastCap Z_R=50 mm h=0.2 mm	TEH2
60	0.991	0.992	0.991	0.928
70	1.230	1.233	1.231	1.194
80	1.389	1.393	1.390	1.368
90	1.508	1.512	1.509	1.493
100	1.606	1.609	1.605	1.594
110	1.690	1.693	1.684	1.674
120	1.767	1.770	1.753	1.746
130	1.834	1.836	1.814	1.810
140	1.889	1.890	1.868	1.867
150	1.948	1.949	1.916	1.917
160	2.003	2.004	1.961	1.963
170	2.055	2.056	2.001	2.006
180	2.103	2.103	2.036	2.048
190	2.143	2.143	2.069	2.087
200	2.192	2.195	2.109	2.124
210	2.225	2.226	2.133	2.159
220	2.261	2.261	2.165	2.192
230	2.297	2.298	2.188	2.223
240	2.331	2.334	2.217	2.252

B.3 Calculations of C_f for the Hartshorn and Ward apparatus (disc-shaped electrode inside reentrant cylinder)

C_f is calculated for Hartshorn and Ward apparatus that is described in Section 2.3.1. The calculations were made with FastCap and FEMM only. The electrodes used are too short to approximate to the infinite length assumed by TEH2. The total capacitance is calculated from which the fringing capacitance is obtained by subtracting the geometric capacitance associated with the side wall and cylinder ends. Residual fringing-capacitance between the reentrant cylinder and the underside of the 'high' electrode is neglected (it is small and can reasonably be assumed to be a part of the constant stray capacitance). Rectangular specimens 54 mm width and 70 mm length are preferred. The specimen width cannot exceed 55 mm, the width of the aperture (Figure 3). The thickness can vary, but 2 mm is normally used. Simulations were used to determine C_f under the following conditions:

- As a function of gap for air-spaced electrodes (Appendix B.3.1).
- For a specimen that is assumed to be circular as a function of diameter (Appendix B.3.2). This gives an indication of how critical the size of specimens is.
- As a function of permittivity for a rectangular specimen of the size normally used for measurement, $70 \times 54 \times 2$ mm, (Section B.3.2). Comparisons with an axisymmetric approximation in which the specimen is assumed to be a disc ⌀70 mm can be made.

Calculations of C_f with FastCap and FEMM can be compared for axisymmetric geometries. These show very good agreement.

B.3.1 With air-spaced electrodes

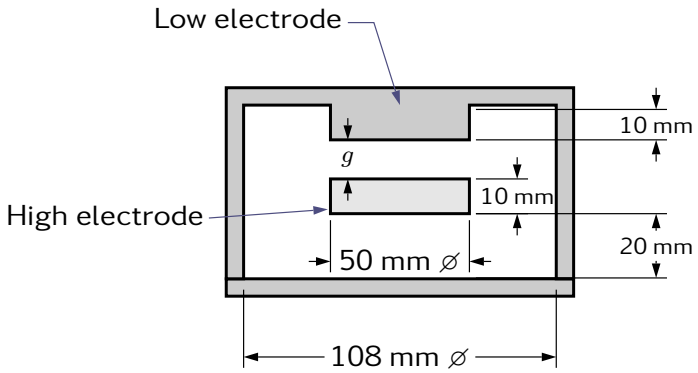

(a): Simplified geometry

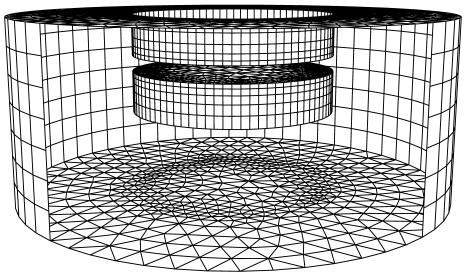

(b): Mesh

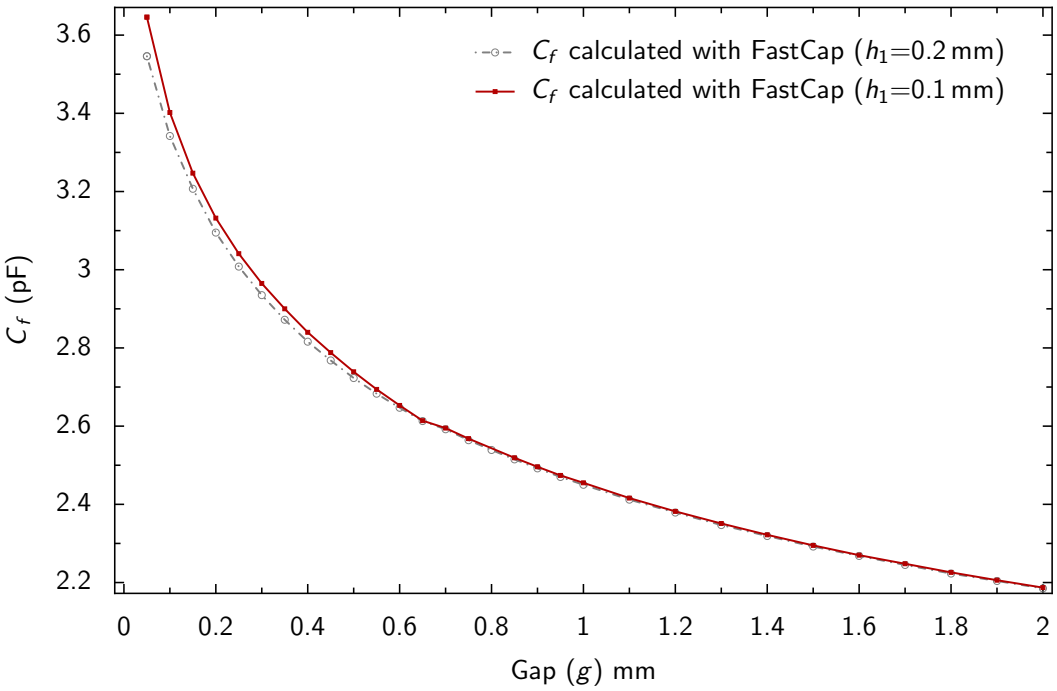

(c): Fringing capacitance calculated with FastCap.

Figure 33: The fringing capacitance C_f for the Hartshorn and Ward apparatus as a function of air gap (no dielectric). C_f was obtained by subtracting the geometric capacitance between the high electrode, and the reentrant cylinder (side wall and two ends) from the total capacitance calculated with FastCap. Residual fringing-capacitance between the 'low' electrode and the underside of the 'high' electrode is neglected as it is comparatively small for the range of gaps shown. The data shown is tabulated in Table 20 (which also includes FEMM calculations).

Table 20: Tabulated values of fringing capacitance calculated with FastCap and FEMM for the Hartshorn and Ward apparatus (Figure 33a) as a function of air gap. FastCap results with mesh parameter h_1=0.05 mm could only be obtained for the smallest gaps.

	C_f (pF)			
Gap g (mm)	FastCap h_1=0.05 mm	FastCap h_1=0.1 mm	FastCap h_1=0.2 mm	FEMM‡
0.05	3.766	3.646	3.546	3.784
0.10	3.482	3.402	3.342	3.459
0.15	3.297	3.247	3.207	3.274
0.20	3.153	3.132	3.095	3.145
0.25	3.037	3.041	3.008	3.047
0.30	2.958	2.965	2.935	2.967
0.35		2.900	2.872	2.900
0.40		2.840	2.816	2.842
0.45		2.788	2.768	2.792
0.50		2.739	2.723	2.747
0.55		2.694	2.683	2.706
0.60		2.653	2.647	2.670
0.65		2.614	2.613	2.636
0.70		2.595	2.592	2.605
0.75		2.568	2.564	2.576
0.80		(Fails)	2.539	2.550
0.85		2.519	2.515	2.524
0.90		2.496	2.492	2.501
0.95		2.474	2.470	2.479
1.00		2.455	2.450	2.458
1.10		2.416	2.412	2.420
1.20		2.382	2.379	2.385
1.30		2.351	2.347	2.353
1.40		2.322	2.319	2.323
1.50		2.295	2.292	2.296
1.60		2.270	2.268	2.272
1.70		2.248	2.245	2.249
1.80		2.226	2.223	2.227
1.90		2.206	2.204	2.207
2.00		2.187	2.185	2.188
2.10		2.168	2.167	2.170
2.20		2.150	2.149	2.153

‡FEMM mesh size 0.02 mm in the vicinity of the electrodes, and 'Auto' elsewhere.

B.3.2 With a disc-shaped specimen, as function of diameter and permittivity

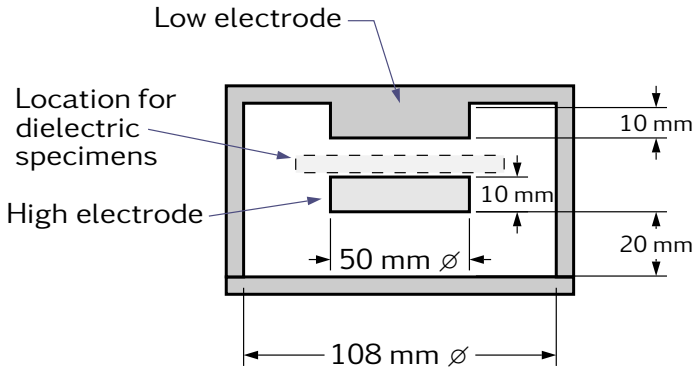

(a): Simplified geometry

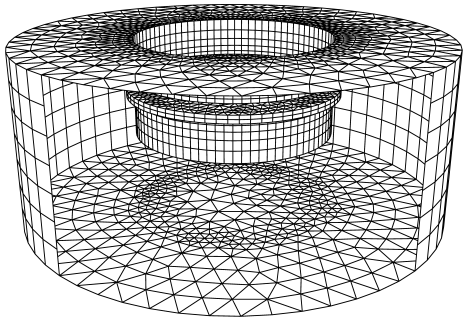

(b): Mesh

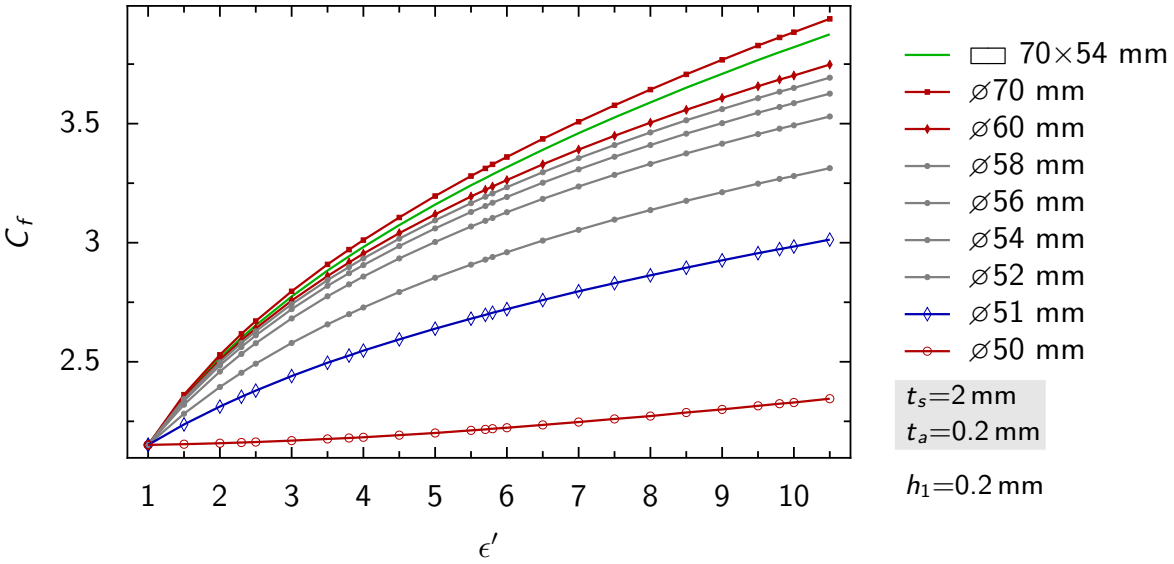

(c): Fringing capacitance calculated with FastCap

Figure 34: The fringing capacitance C_f calculated with FastCap for the Hartshorn and Ward apparatus (Figure 3) with disc-shaped dielectric specimens of varying diameters as a function of permittivity. A set of data for a rectangular specimen 70 × 54 mm (small enough to fit through the specimen entry port) is also shown. In each case, the specimen was 2 mm thick and an air gap above the specimen of 0.2 mm was assumed. The data shown is tabulated in Table 21. Calculations with FEMM give similar results – see Table 22.

Table 21: Tabulated values of fringing capacitance calculated with FastCap for the Hartshorn and Ward apparatus as function of the diameter and permittivity of a dielectric disc. The dimensions used for the calculations are shown in Figure 34. The mesh size parameter was $h_1 = 0.2$ mm. Additional sets of results are provided for a ⌀ 70 mm dielectric disc with the mesh-size parameter reduced to $h_1 = 0.1$ mm, and for a rectangle of dielectric that is small enough to fit through the specimen entry port (Figure 3).

	Diameter of dielectric disc (mm)									Rect. size (mm)
	50	51	52	54	56	58	60	70	70	70 × 54
	Mesh size parameter h_1 (mm)									
	0.2	0.2	0.2	0.2	0.2	0.2	0.2	0.2	0.1	0.2
ϵ'	FastCap C_f (pF)									
1.0	2.151	2.151	2.151	2.151	2.151	2.151	2.151	2.151	2.153	2.151
1.5	2.154	2.237	2.282	2.320	2.336	2.344	2.350	2.362	2.367	2.354
2.0	2.158	2.312	2.394	2.459	2.485	2.498	2.507	2.529	2.537	2.516
2.3	2.161	2.353	2.454	2.533	2.562	2.579	2.590	2.617	2.626	2.601
2.5	2.163	2.379	2.492	2.578	2.611	2.628	2.640	2.671	2.682	2.653
3.0	2.169	2.440	2.579	2.682	2.721	2.742	2.757	2.796	2.810	2.774
3.5	2.176	2.496	2.657	2.775	2.819	2.843	2.860	2.909	2.925	2.883
3.8	2.180	2.526	2.700	2.825	2.872	2.898	2.917	2.971	2.988	2.943
4.0	2.183	2.547	2.728	2.858	2.906	2.934	2.954	3.011	3.030	2.982
4.5	2.192	2.594	2.793	2.934	2.986	3.017	3.040	3.106	3.127	3.074
5.0	2.201	2.639	2.853	3.003	3.060	3.094	3.119	3.196	3.219	3.160
5.5	2.212	2.681	2.908	3.068	3.129	3.166	3.194	3.280	3.305	3.241
5.7	2.216	2.697	2.929	3.092	3.154	3.193	3.222	3.312	3.338	3.271
5.8	2.219	2.706	2.940	3.104	3.168	3.207	3.236	3.329	3.355	3.287
6.0	2.223	2.721	2.960	3.128	3.192	3.233	3.263	3.360	3.387	3.317
6.5	2.235	2.759	3.009	3.184	3.252	3.296	3.329	3.436	3.464	3.390
7.0	2.247	2.796	3.054	3.236	3.308	3.355	3.391	3.508	3.538	3.460
7.5	2.260	2.830	3.097	3.285	3.361	3.410	3.449	3.577	3.609	3.526
8.0	2.272	2.863	3.137	3.331	3.410	3.463	3.504	3.643	3.676	3.589
8.5	2.287	2.895	3.176	3.375	3.458	3.514	3.558	3.707	3.742	3.651
9.0	2.300	2.926	3.212	3.416	3.502	3.561	3.608	3.768	3.804	3.709
9.5	2.315	2.956	3.248	3.456	3.546	3.607	3.657	3.828	3.865	3.767
9.8	2.324	2.973	3.268	3.479	3.570	3.634	3.685	3.862	3.900	3.800
10.0	2.329	2.984	3.280	3.493	3.586	3.650	3.702	3.884	3.922	3.821
10.5	2.345	3.013	3.313	3.530	3.626	3.693	3.748	3.940	3.979	3.875

Table 22: Tabulated values of fringing capacitance obtained by using FEMM for the geometry shown in Figure 34 as a function of the diameter and permittivity (ϵ') of the dielectric disc. These values may be compared to the FastCap results shown in Table 21.

	Diameter of dielectric disc (mm)							
	50	51	52	54	56	58	60	70
	Mesh size 0.02 mm close to electrodes and 'Auto' elsewhere							
ϵ'	FEMM C_f (pF)							
1.0	2.153	2.153	2.153	2.153	2.153	2.153	2.153	2.153
1.5	2.154	2.248	2.292	2.330	2.346	2.354	2.360	2.372
2.0	2.157	2.332	2.413	2.478	2.503	2.517	2.527	2.549
2.3	2.159	2.379	2.479	2.557	2.587	2.603	2.615	2.642
2.5	2.161	2.408	2.520	2.606	2.639	2.657	2.669	2.700
3.0	2.167	2.479	2.616	2.719	2.758	2.780	2.795	2.834
3.5	2.175	2.543	2.703	2.821	2.865	2.890	2.908	2.956
3.8	2.180	2.580	2.752	2.877	2.924	2.951	2.971	3.025
4.0	2.184	2.603	2.783	2.913	2.962	2.990	3.011	3.069
4.5	2.194	2.659	2.856	2.997	3.050	3.082	3.106	3.174
5.0	2.205	2.711	2.923	3.074	3.132	3.167	3.194	3.272
5.5	2.217	2.759	2.985	3.145	3.207	3.246	3.276	3.365
5.7	2.221	2.778	3.009	3.172	3.236	3.276	3.307	3.401
5.8	2.224	2.787	3.020	3.185	3.250	3.291	3.323	3.419
6.0	2.229	2.805	3.043	3.211	3.278	3.320	3.353	3.453
6.5	2.242	2.848	3.097	3.273	3.344	3.389	3.425	3.537
7.0	2.255	2.888	3.147	3.330	3.405	3.454	3.493	3.617
7.5	2.268	2.927	3.194	3.384	3.463	3.516	3.558	3.693
8.0	2.281	2.963	3.238	3.434	3.518	3.574	3.619	3.766
8.5	2.294	2.997	3.280	3.482	3.569	3.629	3.677	3.837
9.0	2.308	3.029	3.319	3.527	3.618	3.681	3.732	3.904
9.5	2.321	3.060	3.356	3.569	3.664	3.731	3.785	3.969
9.8	2.329	3.078	3.377	3.594	3.691	3.759	3.815	4.007
10.0	2.334	3.089	3.391	3.609	3.708	3.778	3.835	4.032
10.5	2.347	3.117	3.424	3.647	3.750	3.823	3.883	4.092

REFERENCES

[1] *ASTM Standard D150, Test methods for AC loss characteristics and permittivity (dielectric constant) of solid electrical insulation*. URL: https://doi.org/10.1520/d0150-18.

[2] *British Standard BS 7663:2018, Methods of test for determination of permittivity and dissipation factor of electrical insulating material in sheet or tubular form*.

[3] R. N. Clarke (Ed.) *Guide to the characterisation of dielectric materials at RF and microwave frequencies*. Tech. rep. The Institute of Measurement, Control, and The National Physical Laboratory, London, 2003. URL: http://eprintspublications.npl.co.uk/id/eprint/2905.

[4] T. M. Minteer. "The many capacitance terms of two parallel discs in free space". In: *European Journal of Physics* 35.3 (Apr. 2014), p. 035022. URL: https://doi.org/10.1088/0143-0807/35/3/035022.

[5] A. C. Lynch. "Edge capacitance in the measurement of dielectric properties". In: *Proceedings of the Institution of Electrical Engineers* 120.8 (1973), pp. 934–938. URL: https://doi.org/10.1049/piee.1973.0208.

[6] G. T. Carlson and B. L. Illman. "The circular disk parallel plate capacitor". In: *American Journal of Physics* 62.12 (Dec. 1994), pp. 1099–1105. URL: https://doi.org/10.1119/1.17668.

[7] G. Paffuti. "Numerical and analytical results for the two discs capacitor problem". In: *Proceedings of the Royal Society A: Mathematical, Physical and Engineering Sciences* 473.2197 (Jan. 2017), p. 20160792. URL: https://doi.org/10.1098/rspa.2016.0792.

[8] *Solutions for measuring permittivity and permeability with LCR meters and impedance analyzers, Application Note 1369-1, Keysight document 5980-2862EN*. 2014.

[9] A. C. Lynch. "Measurement of the dielectric properties of low-loss materials". In: *Proceedings of the Institution of Electrical Engineers* 112.2 (1965), p. 426. URL: https://doi.org/10.1049/piee.1965.0067.

[10] H. S. Endicott. "Guard-gap correction for guarded-electrode measurements and exact equations for the two-fluid method of measuring permittivity and loss". In: *Journal of Testing and Evaluation* 4.3 (May 1976), pp. 188–195. URL: https://doi.org/10.1520/jte10200j.

[11] R. E. Collins and O. R. French. "Design of a guarded electrode". In: *Review of Scientific Instruments* 51.4 (Apr. 1980), pp. 547–548. URL: https://doi.org/10.1063/1.1136234.

[12] B. P. Kibble, J. M. Williams and L. C. A. Henderson (Eds.) *A guide to measuring resistance and impedance below 1 MHz*. Tech. rep. The Institute of Measurement, Control, and The National Physical Laboratory, London, 1999. URL: https://eprintspublications.npl.co.uk/5450/.

[13] A. Kakimoto et al. "Precise measurement of dielectric properties at frequencies from 1 kHz to 100 MHz". In: *Review of Scientific Instruments* 58.2 (Feb. 1987), pp. 269–275. URL: https://doi.org/10.1063/1.1139320.

[14] A. P. Gregory. *Q-factor measurement by using a Vector Network Analyser*. Tech. rep. MAT 58. National Physical Laboratory, 2021. URL: https://doi.org/10.47120/npl.MAT58.

[15] L. Hartshorn and W. H. Ward. "The measurement of the permittivity and power factor of dielectrics at frequencies from 10^4 to 10^8 cycles per second". In: *Journal of the Institution of Electrical Engineers* 79.479 (Nov. 1936), pp. 597–609. URL: https://doi.org/10.1049/jiee-1.1936.0200.

[16] R. Heidinger. *The determination of dielectric parameters of ceramic materials by Q-meter measurements*. Tech. rep. Report KfK 4573. Kernforschungszentrum Karlsruhe, 1989.

[17] A. P. Gregory, G. J. Hill, and M. A. Barnett. "Low loss dielectric measurements in the frequency range 1 to 70 MHz by using a Vector Network Analyser". In: *Meas. Sci. Tech.* (2021). URL: https://doi.org/10.1088/1361-6501/abfd68.

[18] B. Givot et al. "Accurate measurements of permittivity and dielectric loss tangent of low loss dielectrics at frequency range 100 MHz – 20 GHz". In: *2006 International Conference on Microwaves, Radar & Wireless Communications*. IEEE, May 2006. URL: https://doi.org/10.1109/mikon.2006.4345157.

[19] B. Freemire et al. "Low powered RF measurements of dielectric materials for use in high pressure gas filled RF cavities". In: JACoW, Geneva, Switzerland, 2015. URL: http://jacow.org/ipac2015/doi/JACoW-IPAC2015-WEPTY050.html.

[20] J. Baker Jarvis and B. F. Riddle. *Dielectric measurement using a reentrant cavity: a mode matching analysis*. Tech. rep. 1384. 1996. URL: https://doi.org/10.6028/nist.tn.1384.

[21] W. Xi and W. R. Tinga. "Field analysis of new coaxial dielectrometer". In: *IEEE Transactions on Microwave Theory and Techniques* 40.10 (1992), pp. 1927–1934. URL: https://doi.org/10.1109/22.159630.

[22] S. Belomestnykh. "Comment on "Higher order reentrant post modes in cylindrical cavities" [J. Appl. Phys., 144501 (2017)]". In: *Journal of Applied Physics* 123.22 (June 2018), p. 226101. URL: https://doi.org/10.1063/1.5021605.

[23] J. J. Barroso et al. "Analysis and simulation of reentrant cylindrical cavities". In: *International Journal of Infrared and Millimeter Waves* 26.8 (July 2005), pp. 1071–1083. URL: https://doi.org/10.1007/s10762-005-7268-3.

[24] U. Kaatze. "Techniques for measuring the microwave dielectric properties of materials". In: *Metrologia* 47.2 (Mar. 2010), S91–S113. URL: https://doi.org/10.1088/0026-1394/47/2/s10.

[25] H. Hamzah et al. "A compact microwave microfluidic sensor using a re-entrant cavity". In: *Sensors* 18.3 (Mar. 2018), p. 910. URL: https://doi.org/10.3390/s18030910.

[26] *British Standard BS 7737-2:1995, Recommended methods for the determination of the dielectric properties of insulating materials at frequencies above 300 MHz – Resonance methods*.

[27] J. V. L. Parry. “The measurement of permittivity and power factor of dielectrics at frequencies from 300 to 600 Mc/s”. In: *Proceedings of the IEE - Part III: Radio and Communication Engineering* 98.54 (1951), pp. 303–311. URL: https://doi.org/10.1049/pi-3.1951.0062.

[28] J. F. Blackburn. “Measuring dielectric properties using the re-entrant cavity”. NPL internal communication. 2001.

[29] Los Alamos Accelerator Code Group. *Poisson/Superfish [Internet, cited 2021 Sep 5]*. URL: https://laacg.lanl.gov/laacg/services/download_sf.phtml.

[30] A. C. Lynch. “A method for the precise measurement of permittivity of sheet specimens”. In: *Proceedings of the IEE - Part B: Radio and Electronic Engineering* 104.16 (July 1957), pp. 359–362. URL: https://doi.org/10.1049/pi-b-1.1957.0166.

[31] H. El Kamchouchi and A. A. Zaky. “A direct method for the calculation of the edge capacitance of thick electrodes”. In: *Journal of Physics D: Applied Physics* 8.12 (Aug. 1975), pp. 1365–1371. URL: https://doi.org/10.1088/0022-3727/8/12/008.

[32] A. H. Scott and H. L. Curtis. “Edge correction in the determination of dielectric constant, Research Paper RP1217”. In: *Journal of Research of the National Bureau of Standards* 22 (June 1939). URL: https://nvlpubs.nist.gov/nistpubs/jres/22/jresv22n6p747_A1b.pdf.

[33] G. Kirchhoff. “Zur theorie des condensators”. In: *Monatsberichte der Königlich Preußischen Akademie der Wissenschafte zu Berlin* (1877), pp. 48–50. URL: https://doi.org/10.11588/heidok.00013218.

[34] T. E. Hodgetts. *The calculation of the equivalent circuits of coaxial-line step discontinuities*. Tech. rep. Memorandum 3422. Royal Signals and Radar Establishment, 1981. URL: https://apps.dtic.mil/dtic/tr/fulltext/u2/a111962.pdf.

[35] A. P. Gregory et al. *RF and dielectric measurements on layered materials using coaxial sensors*. Tech. rep. MAT 13. National Physical Laboratory, Feb. 2008. URL: http://eprintspublications.npl.co.uk/id/eprint/4075.

[36] A. P. Gregory, R. N. Clarke, and M. G. Cox. “Traceable measurement of dielectric reference liquids over the temperature interval 10–50 °C using coaxial-line methods”. In: *Measurement Science and Technology* 20.7 (June 2009), p. 075106. URL: https://doi.org/10.1088/0957-0233/20/7/075106.

[37] K. Nabors and J. White. “FastCap: a multipole accelerated 3-D capacitance extraction program”. In: *IEEE Transactions on Computer-Aided Design of Integrated Circuits and Systems* 10.11 (1991), pp. 1447–1459. URL: https://doi.org/10.1109/43.97624.

[38] K. Nabors and J. White. “Multipole-accelerated capacitance extraction algorithms for 3-D structures with multiple dielectrics”. In: *IEEE Transactions on Circuits and Systems I: Fundamental Theory and Applications* 39.11 (1992), pp. 946–954. URL: https://doi.org/10.1109/81.199892.

[39] N. Nishimura. “Fast multipole accelerated boundary integral equation methods”. In: *Applied Mechanics Reviews* 55.4 (July 2002), pp. 299–324. URL: https://doi.org/10.1115/1.1482087.

[40] J. Krupka et al. “Uncertainty of complex permittivity measurements by split-post dielectric resonator technique”. In: *Journal of the European Ceramic Society* 21.15 (Jan. 2001), pp. 2673–2676. URL: https://doi.org/10.1016/s0955-2219(01)00343-0.

[41] M. Agustoni and F. Overney. “Impedance Metrology: Bridging the LF–RF Gap”. In: *IEEE Transactions on Instrumentation and Measurement* 70 (2021), pp. 1–8. URL: https://doi.org/10.1109/tim.2020.3036062.

[42] A. M. Shilov et al. “Improved State Primary Special Standard for the Unit of Capacitance in the Frequency Range from 1 to 300 MHz GET 107-2019”. In: *2022 IEEE International Multi-Conference on Engineering, Computer and Information Sciences (SIBIRCON)*. IEEE, Nov. 2022. URL: https://doi.org/10.1109/sibircon56155.2022.10017078.

[43] J. V. Niekerk et al. “Precision differential capacitor”. In: *Precision Engineering* 30.3 (July 2006), pp. 347–352. URL: https://doi.org/10.1016/j.precisioneng.2005.11.011.

[44] J. Schöberl. “NETGEN An advancing front 2D/3D-mesh generator based on abstract rules”. In: *Computing and Visualization in Science* 1.1 (July 1997), pp. 41–52. URL: https://doi.org/10.1007/s007910050004.

[45] K. Nabors et al. *FastCap user’s guide, Research Laboratory of Electronics*. Tech. rep. Massachusetts Institute of Technology Cambridge, MA 02139, 1992.

[46] N.-E. Belhadj-Tahar, O. Dubrunfaut, and A. Fourrier-Lamer. “Broad-band microwave characterization of a tri-layer structure using a coaxial discontinuity with applications for magnetic liquids and films”. In: *IEEE Transactions on Microwave Theory and Techniques* 46.12 (1998), pp. 2109–2116. URL: https://doi.org/10.1109/22.739291.